# Probe spectroscopy in an inhomogeneously broadened three-level system saturated by an intense standing wave

Erkki Kyrölä
*Research Institute for Theoretical Physics, University of Helsinki, Siltavuorenpenger 20C, SF-00170 Helsinki 17, Finland*

Rainer Salomaa
*Nuclear Engineering Laboratory, Technical Research Centre of Finland, P.O.B. 169, SF-00181 Helsinki 18, Finland*
(Received 27 May 1980)

We study inhomogeneously broadened three-level atoms ($\Lambda$ configuration). Two energy levels are strongly coupled by an intense standing wave. A weak laser field at an adjacent transition is used as a probe. The probe response is calculated by Green's functions involving continued fractions. The general solution is extendable to other three-level configurations as well to other types of multimode saturators. The connection of various approximate solutions to the exact one is discussed. We concentrate on the Doppler-free case where both transitions have nearly equal frequencies. For this we derive a reasonably accurate closed-form solution, the parameter dependencies of which are investigated in detail. In addition to its average changes the dynamics of the saturated transition plays an important role in the steady-state probe response. The spectra show sharp resonances which cannot be explained in terms of traveling wave superposition models. The width of the velocity distribution has a strong effect on the shape of the spectrum—some resonances are smeared away because of incomplete Doppler dephasing. The relaxation processes influence differently the resonances, which facilitates their interpretation.

## I. INTRODUCTION

A two-level atom dressed by a strong laser field poses several fundamental questions besides providing a basic theory model for many laser applications. The properties of this system can be studied with the aid of a second laser beam coupled to the same transition (two-level system) or to an adjacent one (three-level system). Both cases have received much attention,[1] but due to the versatility of the nonlinear interactions there has remained many unexplored problems. The probe response in a three-level system saturated by a monochromatic traveling wave (TW) is well understood. The situation changes if the saturator contains several modes or is a standing wave (SW). Because of the nonlinearity, the induced polarization components interfere which gives rise to new spectral features. Undoubtedly the interpretation becomes more complicated, but at the same time one gains in novel well-resolved resonances—let the family of "multiphoton Lamb dips"[2,3] and analogous multiphoton resonances of three-level systems[4,5] serve as examples. To achieve a high enough degree of saturation it may be necessary to place the sample inside the laser cavity; for instance, many infrared double-resonance experiments are performed this way.[6] The SW saturator is also encountered in laser-design problems: One may, e.g., ask when does single-line operation[7] or mode locking[8] occur in lasers capable of oscillating simultaneously in two lines sharing a common level?

A three-level atom interacting with an intense SW saturator and probed by a weak laser field has not been the subject of extensive theoretical efforts. A solution valid for an arbitrary saturator intensity has been derived by Feldman and Feld.[9] The present paper generalizes their model and introduces improved approximate results. Najmbadi *et al.*[7] have discussed the characteristics of two-wavelength lasers within perturbation theory. Besides the intensity restrictions (recently numerical studies in the intense field region have been performed[10]), additional limitations, from the viewpoint of a spectroscopist, are caused by the self-consistency requirements which usually lead to a situation where the various nonlinear processes are not manifested in a best possible way. A homogeneously broadened three-level system can be solved in a closed form.[11] Further support of the present problem is obtained from the multitude of two-level calculations.[12,13] It is also worth pointing out the relationship between our model and the studies on stimulated Raman scattering in atomic-beam configurations.[14] On the other hand, the mathematical formalism to be developed here can be applied to problems like multimode pumping of far infrared and dimer lasers.

An interesting question is how much of the SW configuration can be understood from the basis of simpler saturation models. The superposition of results[15] valid for a co- and counter-running TW saturator is expected to apply for detuned situations only—when do the interference effects become important? A complementary view is obtained by considering the dynamics. Instead of a pure sinusoidal Rabi flipping occurring in TW

 

fields a moving atom experiences a time-dependent saturator in the SW case—how does the modulation in the flipping frequency manifest itself?

In Sec. II we introduce the model atom and field configuration ($\Lambda$ type), and solve the probe response with Green's functions involving continued fractions. Part of the mathematics is deferred to Appendix A. The general solution is rather time consuming and, therefore, various approximations are desirable. These and their qualitative validity conditions are discussed in Sec. III. The subsequent analysis concentrates on the case where the probe and saturator are assumed to have nearly equal frequencies. This is of interest because of the exact cancellation of Doppler shifts. A convenient approximate closed-form solution is introduced in Sec. IV. Some details involved in its velocity averaging are given in Appendix B. The response is split into two terms by their dependence on zero-field population differences ($D^0_{ij} = N^0_i - N^0_j$). In the $D^0_{23}$ term there occurs no average changes in the strongly coupled transition $1 \leftrightarrow 2$ and it thus reflects the dynamics of the dressed $1 \leftrightarrow 2$ system; in the $D^0_{21}$ term additional features appear because of the average polarization and population changes of the transition $1 \leftrightarrow 2$. The parameter dependencies of both contributions are discussed in some detail. The approximate solution of Sec. IV is shown to be quite accurate even for high saturator intensities. If we relax the Doppler-limit approximation the spectra are considerably modified because of the cutoff of the wings of the velocity-dependent spectra. This study allows us to interconnect the homogeneous and inhomogeneous limits. Finally Sec. V gives a summary and discussion of the results.

## II. GENERAL THEORY

We consider the three-level configuration depicted in Fig. 1. The field $\vec{E}_1 = \frac{1}{2}[\vec{E}_1(z)\exp(-i\Omega_1 t) + \text{c.c.}]$ is coupled to the transition $1 \leftrightarrow 2$ and the field $\vec{E}_2$ (with frequency $\Omega_2$) to the adjacent transition $2 \leftrightarrow 3$. The density-matrix elements $\tilde{\rho}_{ij}$ of the system obey within the rotating-wave approximation (RWA) the equations

$$\dot{\rho}_{21} = -[\gamma_{21} + i(\omega_{21} - \Omega_1)]\rho_{21} - i\tilde{\alpha}_1(\rho_{22} - \rho_{11}) + i\tilde{\alpha}_2\rho^*_{13}, \tag{2.1}$$

$$\dot{\rho}_{23} = -[\gamma_{23} + i(\omega_{23} - \Omega_2)]\rho_{23} - i\tilde{\alpha}_2(\rho_{22} - \rho_{33}) + i\tilde{\alpha}_1\rho_{13}, \tag{2.2}$$

$$\dot{\rho}_{13} = -[\gamma_{13} + i(\omega_{13} + \Omega_1 - \Omega_2)]\rho_{13} - i\tilde{\alpha}_2\rho^*_{21} + i\tilde{\alpha}^*_1\rho_{23}, \tag{2.3}$$

$$\dot{\rho}_{11} = \Gamma_1(n^0_1 - \rho_{11}) + \Gamma_{21}\rho_{22} + \kappa_{31}\rho_{33} - 2\,\mathrm{Im}(\tilde{\alpha}^*_1\rho_{21}), \tag{2.4}$$

$$\dot{\rho}_{22} = \Gamma_2(n^0_2 - \rho_{22}) + 2\,\mathrm{Im}(\tilde{\alpha}^*_1\rho_{21} + \tilde{\alpha}^*_2\rho_{23}), \tag{2.5}$$

$$\dot{\rho}_{33} = \Gamma_3(n^0_3 - \rho_{33}) + \Gamma_{23}\rho_{22} + \kappa_{13}\rho_{11} - 2\,\mathrm{Im}(\tilde{\alpha}^*_2\rho_{23}), \tag{2.6}$$

where $\rho_{21} = \tilde{\rho}_{21}\exp(i\Omega_1 t)$, $\rho_{23} = \tilde{\rho}_{23}\exp(i\Omega_2 t)$, $\rho_{13} = \tilde{\rho}_{13}\exp[i(\Omega_2 - \Omega_1)t]$, and $\rho_{ii} = \tilde{\rho}_{ii}$ are assumed to be slowly varying, the dot represents the convective derivative $(\partial/\partial t + v\partial/\partial z)$, and the flipping frequencies are given by

$$\tilde{\alpha}_1 = \vec{\mu}_{21}\cdot\vec{E}_1(z)/2\hbar, \quad \tilde{\alpha}_2 = \vec{\mu}_{23}\cdot\vec{E}_2(z)/2\hbar. \tag{2.7}$$

In this paper we will discuss the case where $\vec{E}_1$ consists of two counter-running waves (SW saturator)

$$\tilde{\alpha}_1 = \alpha_+ e^{iK_1 z} + \alpha_- e^{-iK_1 z} \tag{2.8}$$

and $\vec{E}_2$ is a traveling wave (TW probe)

$$\tilde{\alpha}_2 = \alpha_2 e^{iK_2 z} \tag{2.9}$$

The steady-state solution is obtained as a spatial Fourier series

$$\rho_{ij} = \sum_m \rho_{ij}(m)\exp(imK_1 z) \quad (ij = 11, 22, 33, 21) \tag{2.10}$$

$$\rho_{ij} = \exp(iK_2 z)\sum_m \rho_{ij}(m)\exp(imK_1 z) \quad (ij = 23, 13) \tag{2.11}$$

Insertion of (2.10) and (2.11) into (2.1)–(2.6) yields coupled recurrence relations between the coefficients $\rho_{ij}(m)$.

In the following we simplify the situation by assuming the wave $E_2$ to be a weak probe—the field $E_1$ is allowed to attain an arbitrary intensity. The solution is then given as a perturbation expansion with $\alpha_2$ as a small parameter. To zeroth order, $\rho^{(0)}_{23}$ and $\rho^{(0)}_{13}$ vanish. Formulas for the matrix elements $\rho^{(0)}_{ij}$ of the strongly coupled transition $1 \leftrightarrow 2$ have been derived previously[12] and are reproduced in Appendix A for our readers' convenience (note that $\rho^{(0)}_{33}$ is also modified, because of spontaneous emission and collisional transfer of population).

To first order in $\alpha_2$ we obtain for $\rho_{23}$ and $\rho_{13}$ from (2.2), (2.3), (2.10), and (2.11) the equations

$$\rho_{23}(m) - iL_{23}(m)[\alpha_+\rho_{13}(m-1) + \alpha_-\rho_{13}(m+1)] = -i\alpha_2 L_{23}(m)[\rho^{(0)}_{22}(m) - \rho^{(0)}_{33}(m)], \tag{2.12}$$

$$\rho_{13}(m) - iL_{13}(m)[\alpha^*_+\rho_{23}(m+1) + \alpha^*_-\rho_{23}(m-1)] = -i\alpha_2\rho^{(0)}_{21}(-m)^* \tag{2.13}$$

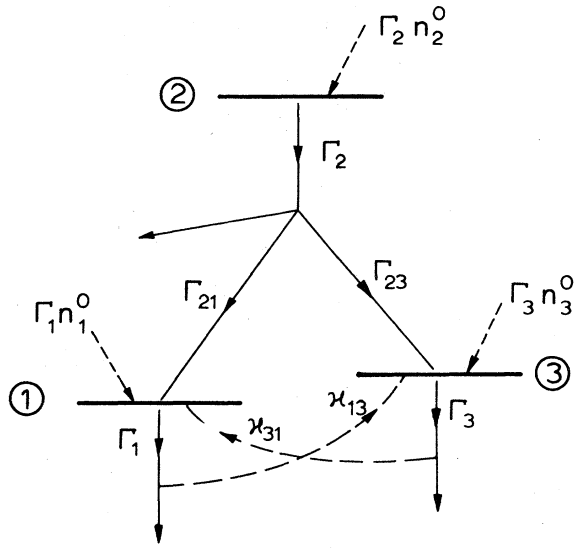


FIG. 1. The model configuration and its relaxation scheme. $\Gamma_{ij}$ describes spontaneous emission, $\kappa_{ij}$ describes collisional transfer of population between the lower levels; phase-changing collisions are included in the off-diagonal decay rates $\gamma_{ij}$. The SW saturator couples to the transition $1 \longleftrightarrow 2$ and the TW probe to $2 \longleftrightarrow 3$. Incoherent pumping is related to the zero-field populations.

(for simplicity we drop the superscript from $\rho_{23}^{(1)}$ and $\rho_{13}^{(1)}$). The complex Lorentzians are defined by

$$L_{23}(m)=[\gamma_{23}+i(\omega_{23}-\Omega_2+K_2v+mK_1v)]^{-1}, \tag{2.14}$$

$$L_{13}(m)=[\gamma_{13}+i(\omega_{13}+\Omega_1-\Omega_2+K_2v+mK_1v)]^{-1}, \tag{2.15}$$

$$L_{21}(m)=[\gamma_{21}+i(\omega_{21}-\Omega_1+mK_1v)]^{-1}. \tag{2.16}$$

Elimination of $\rho_{13}$ leads to the inhomogeneous difference equation

$$a(m)\rho_{23}(m)+b(m)\rho_{23}(m+2)+c(m)\rho_{23}(m-2)=d(m), \tag{2.17}$$

where the coefficients are

$$a(m)=L_{23}^{-1}(m)+\alpha_+^2L_{13}(m-1)+\alpha_-^2L_{13}(m+1), \tag{2.18}$$

$$b(m)=\alpha_-\alpha_+^*L_{13}(m+1), \tag{2.19}$$

$$c(m)=\alpha_+\alpha_-^*L_{13}(m-1), \tag{2.20}$$

and the source term is

$$\begin{aligned} d(m)=&-i\alpha_2[\rho_{22}^{(0)}(m)-\rho_{33}^{(0)}(m)] \\ &+\alpha_2\alpha_+L_{13}(m-1)\rho_{21}^{(0)}(1-m)^* \\ &+\alpha_2\alpha_-L_{13}(m+1)\rho_{21}^{(0)}(-1-m)^* \end{aligned} \tag{2.21}$$

(note that we write $|\alpha|^2=\alpha^2$).

We have solved (2.17) with Green's-function techniques (for details see Appendix A). For the component $\rho_{23}(0)$ which has the right spatial dependence[16] $\exp(iK_2z)$ we find

$$\rho_{23}(0)=G\Big(d(0)+\sum_{m=-2}^{-\infty}S_-(-2)S_-(-4)\cdots S_-(m)d(m) +\sum_{m=2}^{\infty}S_+(2)S_+(4)\cdots S_+(m)d(m)\Big), \tag{2.22}$$

where the descending and ascending continued fractions are defined by the recurrence relations

$$S_-(m)=-c(m+2)[a(m)+b(m-2)S_-(m-2)]^{-1}, \tag{2.23}$$

$$S_+(m)=-b(m-2)[a(m)+c(m+2)S_+(m+2)]^{-1}, \tag{2.24}$$

and the Green's function $G=G(0,0)$ is given by

$$G=[a(0)+c(2)S_+(2)+b(-2)S_-(-2)]^{-1}. \tag{2.25}$$

The probe absorption (dispersion) is obtained from the imaginary (real) part of $\rho_{23}(0)$ in the usual manner.[17]

The probe response has already been derived by Feldman and Feld.[9] We have preferred the Green's-function techniques to their variational approach. Besides this technical difference our model is more flexible in the choice of field and relaxation parameters. Instead of a pure SW saturator[18] we allow arbitrary values for the amplitudes $\alpha_+$ and $\alpha_-$; one advantage obtained is that pure TW effects are readily extracted by letting either $\alpha_+$ or $\alpha_-$ disappear and there is no need to go to the off-resonant limit. We can also easily distinguish interference terms by keeping track of products of $\alpha_+^2$ and $\alpha_-^2$. The general relaxation scheme adopted facilitates the tracing of various contributions like those due to $\rho_{13}$ coherence. We have kept $\gamma_{ij}\geq\frac{1}{2}(\Gamma_i+\Gamma_j)$ as free parameters and included both spontaneous decay from level 2 to levels 1 and 3 and collisional population exchange between levels 1 and 3. (The model is, of course, oversimplified to give a full account of collisional effects.[19])

It is convenient to divide the terms appearing in $\rho_{23}$ according to their dependence on the field-free population differences $D_{ij}^0$ between the levels $i$ and $j$. This term classification has been used before[9] and can be realized experimentally by properly adjusting the incoherent pumping rates.[2] According to (A21) and (2.21) we have

$$\begin{aligned} d(m)=&-i\alpha_2D_{23}^0\delta_{m,0}-i\alpha_2f(m)[D_{21}(m)-D_{21}^0\delta_{m,0}] \\ &+\alpha_2\alpha_+L_{13}(m-1)\rho_{21}^{(0)}(1-m)^* \\ &+\alpha_2\alpha_-L_{13}(m+1)\rho_{21}^{(0)}(-1-m)^*, \end{aligned} \tag{2.26}$$

where the function $f(m)$ is defined by (A22) and $D_{21}(m)=\rho_{22}^{(0)}(m)-\rho_{11}^{(0)}(m)$. The first term multi-

plied by the Green's function $G$ in (2.22) gives rise to the $D^0_{23}$ term.

If we have $D^0_{21}=0$, the saturator does not induce any average polarization or population changes in the strongly coupled transition $1 \leftrightarrow 2$. The response is entirely due to the $D^0_{23}$ term. At first it is somewhat embarassing that this term (called also a light shift[2] or background signal) still depends on the saturator. To understand this one must ponder the dynamics of the strongly coupled system. An atom originally created onto level 2 (or 1) experiences Rabi flipping which the probe field is able to feel. As regards the saturated transition the upward and downward flipping rates cancel and no net changes in the populations of levels 1 and 2 occur. The probe transition, however, is selective to the probability amplitude of the common state 2 and thus it matters in what state the atom enters. The periodic modulation is included in the Green's function $G$ which represents an effective propagator $\rho_{23} \to \rho_{13} \to \rho_{23}$ in the frequency space. Its poles give the eigenfrequencies of the dressed system $2 \leftrightarrow 3$.

The $D^0_{21}$ term contains both a population [second term in (2.26)] and polarization-induced contribution ($\sim\rho^{(0)}_{21}$), which can be partly distinguished by their relaxation or detuning dependence. The Green's function $G$ enters the $D^0_{21}$ term, too, because in excitation chains like $\to\rho_{22}\to\rho_{23}\to$ or $\to\rho_{21}\to\rho_{13}\to\rho_{23}\to$ the dynamics of $\rho_{23}$ is determined by $G$. A loose classification is preferred here because various low-intensity processes like stepwise and Raman-type transitions interfere strongly in the high-intensity region.

Equation (2.22) is readily evaluated numerically. Rather long computing times are, however, needed. Furthermore, the complexity of the equations tend to obscure the underlying physics and hamper the extraction of parameter dependencies. Some simpler closed-form approximations are, therefore, desirable. These are discussed in the following sections.

## III. APPROXIMATE SOLUTIONS AND THEIR RELATIONSHIP

As in the corresponding case of probing a strongly coupled two-level system,[13] the full solution (2.22) can be expressed in a closed form in a few special situations only. For stationary atoms ($v=0$) the continued fractions $S_\pm(m)$ [as also those of the strongly coupled system, see (A13) and (A14)] become periodical which permits us to calculate them exactly. The infinite sums in (2.22) reduce to geometric series and are easily performed. We have checked that Eq. (2.22) indeed reproduces the previously given formulas.[11] The continued fractions and infinite sums in (2.22) are exactly truncated for a TW saturator ($\alpha^2_+\alpha^2_- = 0$). A third exception which leads to a closed-form solution arises when we have a resonant SW saturator, and in the relaxation scheme adopted by Feldman and Feld[9] the restriction $\Gamma_1=\Gamma_2$ is made. The result can then be expressed as a ratio between complex-order Bessel functions. The special cases above provide convenient check points for numerical computations and approximate formulas.

In general, the summation in (2.22) can be cut off once the product of the continued fractions $S_\pm(m)$ and the source terms $d(m)$, which depend on the continued fractions of the strongly coupled transition $1 \leftrightarrow 2$, becomes small enough. The convergence of $S_\pm(m)$ can be inspected by carrying out an equivalence transformation in them. The emerging convergence factor turns out to be

$$\xi(m)= b(m)c(m+2)/a(m)a(m+2)\,. \tag{3.1}$$

According to (2.18)–(2.20) the magnitude of this is roughly determined by the product $\alpha^2_+\alpha^2_- |L_{13}|^2 \times |L_{23}|^2$ (for simplicity we drop the index $m$). The following possibilities enter.

(i) $\alpha^2_+=0$ or $\alpha^2_-=0$, i.e., we have a pure TW saturator.

(ii) $\alpha^2_+\alpha^2_-$ is small which justifies a perturbation expansion in terms of the interference terms of the saturator components [a kind of independent-field approximation (IFA)]. If $\alpha^2_+$ and $\alpha^2_-$ are also assumed to be small we obtain the ordinary perturbation solution.

(iii) $|L_{13}|^2$ is small, i.e., $\rho_{13}$ coherence is negligible. This occurs, e.g., when $\gamma_{13}\to\infty$ or far off from the "two-photon" resonances. The modulation of the population $\rho_{22}$ is the dominant effect as has been discussed by Feldman and Feld[9] (we prefer to reserve the term IFA for case ii above). If we furthermore neglect the spatial variations of $\rho_{22}$ (let $\alpha^2_+\alpha^2_-\to 0$) we obtain the familiar rate-equation approximation (REA).

(iv) $|L_{23}|^2$ may be small because of a large value of $\gamma_{23}$ or a detuned intermediate level. This case is of minor spectroscopical interest except near the two-photon resonances (Raman-type processes).

(v) By a proper choice of the probe and saturator detuning we may avoid the overlap of resonances due to $L_{13}$ and $L_{23}$ and thus keep the product $|L_{13}L_{23}|$ small (cf. iii and iv).

The magnitude of $\xi(m)$ does not, however, solely determine the accuracy of the approximation chosen. In the velocity integration (especially in the Doppler limit) many seemingly large terms may disappear and the model turn out to be much better than expected.

Although the formulas of Sec. II have been derived for a general $\Lambda$ configuration, and can be extended to cover $V$ and cascade configurations too, we want to restrict the parameter analysis. Of special interest is the situation $K_1 \simeq K_2 = K$ in which Doppler shifts are exactly cancelled in Raman-type processes. In the following section we introduce a novel approximation for this special case which considerably improves the population sensing model (case iii above) of Feldman and Feld.[9] In this we retain the Doppler-free Lorentzian $L_{13}(-1)$, but neglect all other functions $L_{13}(m)$. This becomes partly justified by noting that only a narrow velocity group satisfies the resonance conditions arising from $L_{13}(m)$ whereas all atoms contribute to $L_{13}(-1)$.

## IV. DOPPLER-FREE (QUADRUPLE-COHERENCE) APPROXIMATION (DFA)

### A. Derivation and general characteristics

With the assumption $L_{13}(m) = L_{13}\delta_{m,-1}$ Eq. (2.22) reduces to $[\rho_{23} = \rho_{23}(0)]$:

$$\rho_{23} = G\left(d(0) + \frac{\alpha_+\alpha_-^* L_{13}}{L_{23}^{-1}(-2) + \alpha_-^2 L_{13}} d(-2)\right), \tag{4.1}$$

where $G$, $d(0)$, and $d(-2)$ are now given by

$$G = \{L_{23}^{-1}(0) + \alpha_+^2 L_{13}[1 + \alpha_-^2 L_{13} L_{23}(-2)]^{-1}\}^{-1}, \tag{4.2}$$

$$d(0) = -i\alpha_2 D_{23}(0) + \alpha_2\alpha_+ L_{13}\rho_{21}^{(0)}(1)^*, \tag{4.3}$$

$$d(-2) = -i\alpha_2 D_{23}(-2) + \alpha_2\alpha_- L_{13}\rho_{21}^{(0)}(1)^*. \tag{4.4}$$

The population difference $D_{23}(m) = [\rho_{22}^{(0)}(m) - \rho_{33}^{(0)}(m)]$ and the off-diagonal component $\rho_{21}^{(0)}(m)$ are the zeroth-order perturbation solutions in the probe amplitude [see (A19) and (A21)]. The source terms $D_{23}$ and $\rho_{21}^{(0)}$ still contain continued fractions. To further simplify the calculations we adopt the REA solution for the strongly coupled transition $1 \rightarrow 2$, i.e., we take $D_{21}(m) = D_{21}(0)\delta_{m,0}$. This, together with the assumption $L_{13}(m) = L_{13}\delta_{m,-1}$, is equivalent to making a RWA in (2.1)–(2.6) with respect to the phasors $\exp(imKz)$ with $|m| \geq 2$ (in the rest frame of the atom a RWA in the radio-frequency domain). From Eqs. (4.1)–(4.4), (A19), and (A21) we find

$$\rho_{23} = -i\alpha_2 G\{D_{23}^0 + f[D_{21}(0) - D_{21}^0] + i\alpha_+\rho_{21}^{(0)}(1)^* L_{13}[1 + \alpha_-^2 L_{13}(L_{23}^{-1}(-2) + \alpha_-^2 L_{13})^{-1}]\}, \tag{4.5}$$

where

$$D_{21}(0) = D_{21}^0\{1 + 2g[\alpha_+^2 \mathrm{Re}L_{21}(1) + \alpha_-^2 \mathrm{Re}L_{21}(-1)]\}^{-1}, \tag{4.6}$$

$$\rho_{21}^{(0)}(1) = -i\alpha_+ L_{21}(1) D_{21}(0), \tag{4.7}$$

and $G$ is given by (4.2). The quantities $f = f(0)$ and $g = g(0)$ are defined by (A22) and (A18), respectively. In the following we neglect collisional transfer of population between levels 1 and 3 ($\kappa_{13} = \kappa_{31} = 0$) and have

$$g = (\Gamma_1 + \Gamma_2 - \Gamma_{21})/\Gamma_1\Gamma_2, \tag{4.8}$$

$$fg = (\Gamma_3 - \Gamma_{23})/\Gamma_2\Gamma_3. \tag{4.9}$$

[Note that after insertion of (4.6) into (4.5) only the product $fg$ remains.]

We call the approximation scheme leading to Eq. (4.5) Doppler-free (quadruple-coherence) approximation (DFA). The velocity average of $\rho_{23}$ (denoted by brackets $\langle \rho_{23} \rangle$) is easily performed numerically; analytical results valid in the Doppler limit are derived in Appendix B. For a TW saturator Eq. (4.5) reproduces the probe response exactly in the co-running case ($\alpha_-^2 = 0$), but gives only the REA-type expression in the counter-running configuration ($\alpha_+^2 = 0$). This could be remedied by retaining the Lorentzian $L_{13}(1)$ in addition to $L_{13}(-1)$; this kind of independent-field approximation is used, e.g., in Ref. 20. The IFA of Feldman and Feld[9] follows from (4.1) by letting $L_{13} \rightarrow 0$ when $\rho_{23} \rightarrow -i\alpha_2 L_{23}(0) D_{23}(0)$; then the full structure (note the REA made in the DFA) of the population difference $D_{23}(0)$ is scanned by the simple Lorentzian $L_{23}(0)$ replacing the Green's function (4.2).

### B. Propagator $G(v)$

It turns out that many of the features observed in the probe spectra are caused by the Green's function $G$, which thus, is worth a more detailed analysis. In the low-intensity limit $G(v)$ reduces to the simple Lorentzian $L_{23}(0)$ centered at $Kv = -\Delta_{23}$. Higher-order expansions of the exact $G(v)$, Eq. (2.25), contain products of the Lorentzians $L_{13}(p)$ ($p$ is odd) and $L_{23}(m)$ ($m$ is even). The requirement that the respective resonant velocity groups coincide leads to the general resonance condition $l\Delta_{23} = k\Delta_{21}$ where $k$ and $l$ are arbitrary odd integers and

$$\Delta_{23} = \omega_{23} - \Omega_2, \quad \Delta_{21} = \omega_{21} - \Omega_1. \tag{4.10}$$

Contributions of various orders can overlap: For instance, the pairs $\{L_{23}(0), L_{13}(-3)\}$ and $\{L_{23}(2), L_{13}(-7)\}$ both give rise to a resonance at $\Delta_{23} = \Delta_{21}/3$ which, indeed, appears in some of the spectra; also when $\Delta_{23} = 0$ or $\Delta_{23} = \Delta_{21}$ all $L_{23}(m)$ and $L_{13}(m)$, respectively, are "resonant" for $v = 0$. For intense saturators one, therefore, should expect a

quasicontinuum of multiphoton resonances. The heights and shapes of the corresponding peaks depend on the order of the process and also on how they survive the velocity averaging. In fact only a finite number of observable extrema remains in the probe spectrum, and even if one were able to label a certain peak, large power deformations (shifts, broadening, and splitting) in it must be accounted for.

A perturbation analysis of the approximate $G(v)$, Eq. (4.2), suggests just the two resonances $\Delta_{23}=0$ and $\Delta_{23}=\Delta_{21}$. Instead of this we study its poles (and the corresponding residues). In the complex velocity space these are located at[21]

$$Kv=\pm(\Delta_{23}-i\gamma_{23})[1+(\alpha_+^2+\alpha_-^2)L_{13}L_{23} + \tfrac{1}{4}(\alpha_+^2-\alpha_-^2)^2L_{13}^2L_{23}^2]^{1/2} + \tfrac{1}{2}i(\alpha_+^2-\alpha_-^2)L_{13}, \quad (4.11)$$

where $L_{23}=(\gamma_{23}+i\Delta_{23})^{-1}$. If we have a SW saturator, i.e., $\alpha_+^2=\alpha_-^2=\frac{1}{4}\alpha^2$, Eq. (4.11) simplifies to

$$Kv=\pm(\Delta_{23}-i\gamma_{23})(1+\tfrac{1}{2}\alpha^2L_{13}L_{23})^{1/2}. \quad (4.12)$$

By neglecting the decay rates for a moment, we see that (4.12) attains purely imaginary values in the detuning ranges

$$\tfrac{1}{2}\Delta_{21}-\tfrac{1}{2}(\Delta_{21}^2+2\alpha^2)^{1/2}\le\Delta_{23}\le\min\{0,\Delta_{21}\}, \quad \max\{0,\Delta_{21}\}\le\Delta_{23}\le\tfrac{1}{2}\Delta_{21}+\tfrac{1}{2}(\Delta_{21}^2+2\alpha^2)^{1/2}. \quad (4.13)$$

The absence of resonance atoms indicates a decrease of the probe response.[22] For small values of $\Delta_{21}$ one must take into account the decay rates $\gamma$ in the vicinity of $\Delta_{23}=0$ and therefore (4.13) is inapplicable. Equation (4.12), too, suggests that appreciable structure may appear near this point because then the corresponding velocity groups partly overlap.

Calculations[15,23] for TW saturators predict the resonance groups (for simplicity put $\gamma_{ij}=0$)

$$Kv=-\Delta_{23}+\alpha^2/(\Delta_{23}-\Delta_{21}) \quad (4.14)$$

for the co-running case ($\alpha_+^2=\alpha^2, \alpha_-^2=0$) and

$$Kv=-\tfrac{1}{4}(3\Delta_{23}-\Delta_{21}) \pm\tfrac{1}{4}[(\Delta_{23}+\Delta_{21})^2+8\alpha^2]^{1/2} \quad (4.15)$$

for the counter-running case ($\alpha_+^2=0, \alpha_-^2=\alpha^2$). Equation (4.11) reproduces (4.14), but gives only $Kv=-\Delta_{23}$ instead of (4.15). Owing to the neglect of the Lorentzian $L_{13}(1)$ the approximate $G(v)$ fails near $2Kv\simeq\Delta_{21}-\Delta_{23}$. Note also that in contrast to (4.13) in the TW models resonance groups always exist, although very large shifts in (4.14) may take place for $\Delta_{23}\simeq\Delta_{21}$.

Figure 2 displays the exact Green's function (2.25) and the approximation (4.2) for a resonant SW saturator. The representative values chosen for $\Delta_{23}$ are indicated in Fig. 3 which gives the velocity-averaged response ($D_{23}^0$ term, see Sec. IV C). The DFA result is a Lorentzian-like curve slightly power shifted from the center point $Kv=-\Delta_{23}$; the structure near the symmetric point $Kv=\Delta_{23}$ is almost negligible. Large power broadening which in fact is due to splitting [cf. (4.12)] occurs when we have $\Delta_{23}=\Delta_{21}=0$. In the exact Green's function the two-photon peak at $Kv\simeq\frac{1}{2}(\Delta_{21}-\Delta_{23})$ due to $L_{13}(1)$ is clearly seen; higher-order multiphoton resonances give rise to the fine structure near $Kv\simeq 0$. Except when these strongly overlap with the dominant peak at $Kv\simeq-\Delta_{23}$, their integrated area almost vanishes as is indicated by

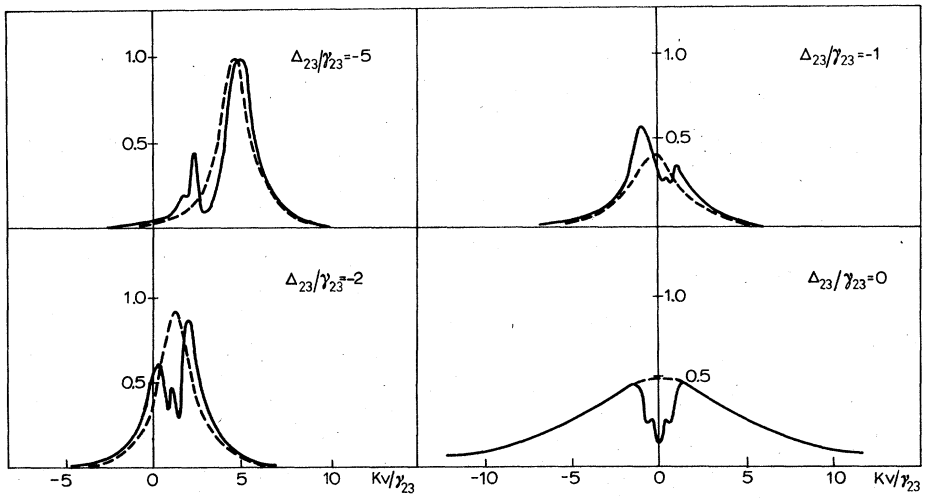


FIG. 2. The velocity dependence of the Green's function (in units of $\gamma_{23}^{-1}$) according to the exact formula (2.25) (solid line) and the DFA [Eq. (4.2), broken line] at various probe detunings $\Delta_{23}$. A resonant ($\Delta_{21}=0$) SW saturator with $\alpha^2=5\gamma_{23}^2$ is assumed; $\gamma_{13}=0.1\gamma_{23}$.

the accuracy of the DFA in Fig. 3 (cf. the sum rules[24]). The dip appearing at $Kv=0$, for $\Delta_{23}\simeq 0$ becomes important when the width of the velocity distribution is decreased as will be demonstrated in Sec. IV D. Note also how the peak heights are reduced in the case $\Delta_{23}=-\gamma_{23}$ which roughly satisfies the condition (4.13).

If we have a detuned saturator, Figs. 4 and 5, the various resonances are more easily distinguishable because of weaker interference between them. The main feature of $G(v)$ is still the (slightly) power-distorted peak at $Kv=-\Delta_{23}$. This and the narrow resonance at $Kv=\frac{1}{2}(\Delta_{21}-\Delta_{23})$ (absent in the DFA) overlap for $\Delta=-\Delta_{21}$ which explains the split spectrum in the case $\Delta_{23}=-15\gamma_{23}$. According to (4.13) no resonant atoms are found if $\Delta_{23}/\gamma_{23}$ falls in the range $(-1.5, 0)$ or $(15, 16.5)$. Indeed in the cases $\Delta_{23}/\gamma_{23}=-1.6$ and 16.6 the reduction in the probe response is visible in both Figs. 4 and 5. Again some fine structure due to multiphoton processes develops (mainly near $Kv\simeq 0$) when $\Delta_{23}\simeq 0$ or $\Delta_{21}$. The only one that clearly survives the velocity integration is the $\Delta_{21}/3$ dip visible at $\Delta_{23}\simeq 4.4\gamma_{23}$ in Fig. 5 (note the splitting of the corresponding curve in Fig. 4). The interference is strongest near $\Delta_{23}=\Delta_{21}$. Very large shifts and broadening take place in $G(v)$; in the vicinity of the maximum at $\Delta_{23}\simeq 14.9\gamma_{23}$ $G(v)$ is extremely flat when this peak is easily smeared away if its wings are cut off by a Gaussian velocity distribution. On the contrary, the maximum at $\Delta_{23}\simeq 17.6\gamma_{23}$ is affected to a much lesser extent.

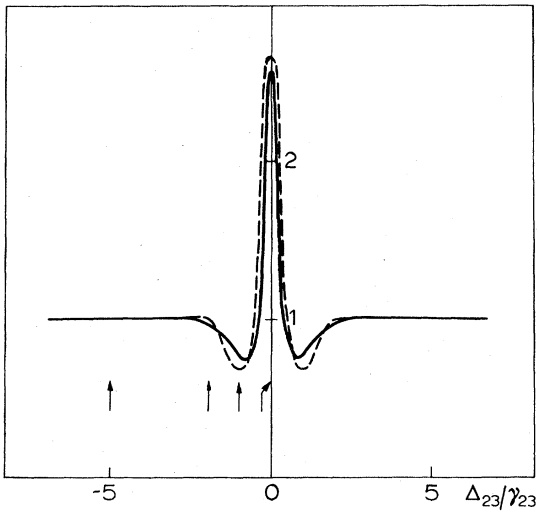


FIG. 3. The velocity integral of Re($G$) (arbitrary units) in the Doppler limit (the broken line gives the DFA result). The arrows indicate the probe detunings corresponding to Fig. 2.

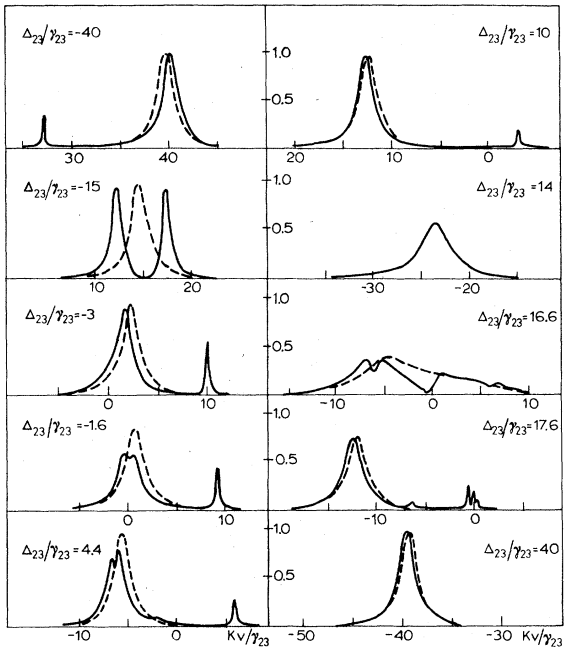


FIG. 4. The same as Fig. 2 but with $\Delta_{21}=15\gamma_{23}$ and $\alpha^2=50\gamma_{23}^2$. Only the main portions of Re($G$) are displayed (note the changes in the abscissa axis).

### C. $D_{23}^0$ term

If the incoherent pumping rates are chosen such that $D_{21}^0=0$, only the term proportional to $D_{23}^0$ in (4.5) contributes. It gives the ordinary Voigt profile of the transition $2\leftrightarrow 3$ in the limit $\alpha_\pm^2\to 0$. We also want to remind our readers that it is just the velocity average of the Green's function $G(v)$. In

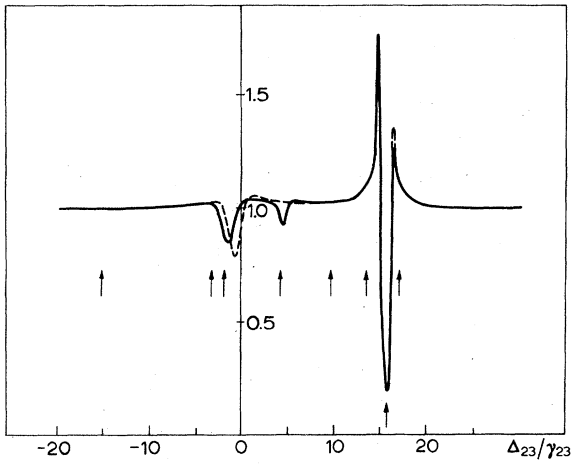


FIG. 5. Integrated spectrum Re ($\langle G\rangle$) corresponding to Fig. 4. Probe detunings selected in Fig. 4 are denoted by the arrows.

the Doppler limit we find

$$\langle \rho_{23} \rangle = \frac{i\alpha_2 \pi^{1/2}}{Ku} D_{23}^0 [1 + \tfrac{1}{16}\alpha^4 L_{13}^2 L_{23}^2 (1 + \tfrac{1}{2}\alpha^2 L_{13} L_{23})^{-1}]^{1/2} \tag{4.16}$$

for a SW saturator (see Appendix B).

Figures 6 and 7 display the absorptive part of (4.16) for various saturator intensities. In the resonant case ($\Delta_{21}=0$) the most prominent feature is the peak occuring at $\Delta_{23}=0$. Its shape is given by $\mathrm{Re}(L_{23}^2 L_{13}^2)$ in the limit $\alpha^2 \to 0$ and by $\mathrm{Re}[(L_{23}L_{13})^{1/2}]$ when $\alpha^2 \to \infty$ (a pure Lorentzian if $\gamma_{13}=\gamma_{23}$). Thus in both limits neither power broadening nor power shifts are present. The width equals roughly $\min\{\gamma_{23}, \gamma_{13}\}$. The peak height is given by

$$\mathrm{Im}(\langle \rho_{23} \rangle) = \frac{\alpha_2 \pi^{1/2}}{Ku} D_{23}^0 \left(1 + \frac{\alpha^4/16\gamma_{13}^2\gamma_{23}^2}{1 + \alpha^2/2\gamma_{13}\gamma_{23}}\right)^{1/2}. \tag{4.17}$$

The relevant dimensionless saturation parameter is, hence, $\alpha^2/\gamma_{13}\gamma_{23}$. As $\alpha^2$ is increased the growth of the maximum value slows down from $\alpha^4$ to $\alpha$ but does not saturate to a constant value. For very large $\alpha^2$ one should not, however, rely on the DFA and, furthermore, the Doppler-limit approximation is expected to fail.

Excluding the central peak at $\Delta_{23}=0$ the regions of weak absorption are readily explained by (4.13). The side maxima having approximately the width $\frac{1}{2}(\gamma_{13}+\gamma_{23})$ appear at $\Delta_{23} \simeq \pm(\alpha^2/2)^{1/2}$. Their height increases only as $\alpha^{1/2}$ in the limit $\alpha \to \infty$ which makes the contrast of the central peak even larger. Their apparent dispersive shape actually results from a square root of a complex Lorentzian [see (B7)]. If $\alpha^2$ changes either spatially or (slowly) in time, the side maxima move and are partly averaged out of the integrated response.

For an off-resonant saturator the probe spectrum has its main variation near the points $\Delta_{23}=0$, $\Delta_{23}=\Delta_{21}$, and $\Delta_{23}=\frac{1}{2}\Delta_{21} \pm \frac{1}{2}(\Delta_{21}^2 + 2\alpha^2)^{1/2}$ according to Eq. (B4) (note that this structure does not appear in Ref. 9). Again the regions of weak absorption are explained by (4.13). When intermediate saturator intensities are applied the resonance shapes are approximately square roots of Lorentzians and the relevant interaction parameter equals $\alpha^2/|\Delta_{21}|\gamma$ where $\gamma$ is either $\gamma_{13}$ or $\gamma_{23}$ depending on the peak considered. This is evidenced by the asymmetry of the curves with $\gamma_{13}=0.1\gamma_{23}$ in Fig. 7 (note also the widths). All four maxima experience power shifts as also shifts due to the skewed background caused by the nearby peaks, but they are only modestly saturated and power broadened. The variations of $\alpha^2$ affect less the averaged innermost maxima than the outer ones. The detuning dependence of the $D_{23}^0$ term is qualitatively summarized in Fig. 8.

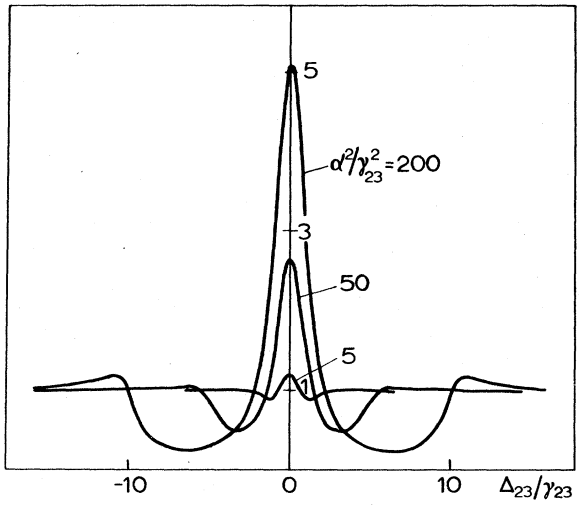


FIG. 6. Imaginary part of the $D_{23}^0$ term (probe absorption spectrum when the zero-field populations of the strongly coupled levels 1 and 2 are equal) in arbitrary units at various saturator intensities according to DFA. A resonant saturator is assumed; $\gamma_{13}=\gamma_{23}$.

### D. Effects due to finite Doppler widths, accuracy of the DFA

In practice the velocity distribution (here we assume a Gaussian $\exp(-v^2/u^2)/\pi^{1/2}u$) has a finite width. The observed probe spectra may, therefore, considerably differ from those predicted by formulas based on the Doppler-limit approximation, e.g., Eq. (4.16). This is illustrated in Figs. 9 and 10. A comparison between these and Figs. 3 and 5 reveals that some resonances are completely smeared out. To understand this one has to know how the Green's function $G(v)$ depends on the saturator and to remember that the Gaussian velocity distribution weighs the contribution of

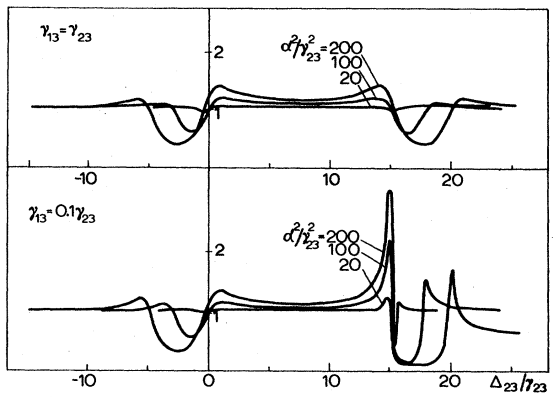


FIG. 7. The same as Fig. 6. but with $\Delta_{21}=15\gamma_{23}$ and two different values for $\gamma_{13}$.

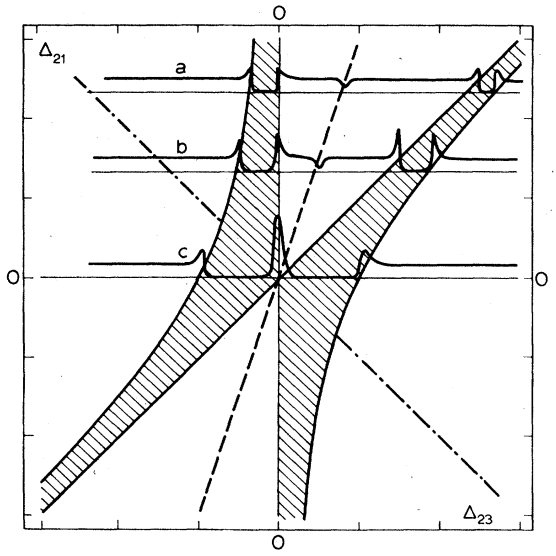


FIG. 8. This figure illustrates the qualitative behavior of the $D_{23}^0$ term. The horizontal line both gives the zero level of absorption and indicates the saturator detuning. In the shaded region determined by (4.13) resonant atoms are absent. Two examples of perturbation theoretical resonance predictions are shown, too: In the case $\Delta_{23} = \Delta_{21}/3$ (broken line) a dip appears, but in the case $\Delta_{23} = -\Delta_{21}$ (dash-dotted line) the emerging structure is negligible.

atoms with slow velocities ($|v| \lesssim u$). The width of the Gaussian also determines how much of the extra structure absent in the approximate Green's function is integrated away (cf. Sec. IV B) and thus directly influences the accuracy of the DFA.

Let us first consider a resonant saturator for which case the Green's function is illustrated in Fig. 2. We already mentioned that the structure of $G(v)$ which the DFA is unable to repeat has almost zero area when $\Delta_{23} \neq 0$ and, therefore, the DFA is expectedly quite accurate for large Doppler widths $Ku$. Near the resonance $\Delta_{23} = 0$ the values of $G(v)$ around $Kv = 0$ become the more important the smaller $Ku$ is. DFA underestimates the saturation of the probe response [e.g., the neglect of $L_{13}(1)$ is not justified for $Kv = 0$] which explains its wrong behavior in Fig. 9. Note also that the Gaussian cuts off the wings of $G(v)$ in just those regions where DFA is reasonably good. According to (4.12) the width $K\delta v$ of the resonant velocity group is approximately $(\gamma_{23}^2 + \alpha^2\gamma_{23}/\gamma_{13})^{1/2}$, i.e., ca. $5\gamma_{23}$ for the parameters of Fig. 9. That $Ku$ has to exceed $K\delta v$ gives one criterion for the applicability of the DFA and indeed it is quite satisfactory already when $Ku = 10\gamma_{23}$.

As Fig. 9 shows, the central dip of the homogeneous case turns over to a maximum as $Ku$ is increased. Analogous modifications occur also for a detuned saturator (Fig. 10). The most prominent one is the disappearance of the sharp maximum in Fig. 5 at $\Delta_{23} \simeq 14.9\gamma_{23}$ as $Ku$ is decreased. This is readily explained by the excessive broadening of $G(v)$ in this parameter range (see Fig. 4). In other detuning regions $G(v)$ just experiences modest shifts and broadening when the magnitude of the Doppler width has only a minor effect on the accuracy of the DFA. The additional structure present in the exact $G(v)$ is again efficiently integrated out (zero-area property). A rather large value of $Ku$ is required before the $\Delta_{21}/3$ dip, primarily due to the Lorentzian $L_{13}(-3)$, becomes visible. In experiments this kind of small structure may completely disappear because of noise and variations of laser parameters.

Figures 9 and 10 demonstrate that the DFA is remarkably good even for the rather high saturator intensities chosen [note that usually one has to per-

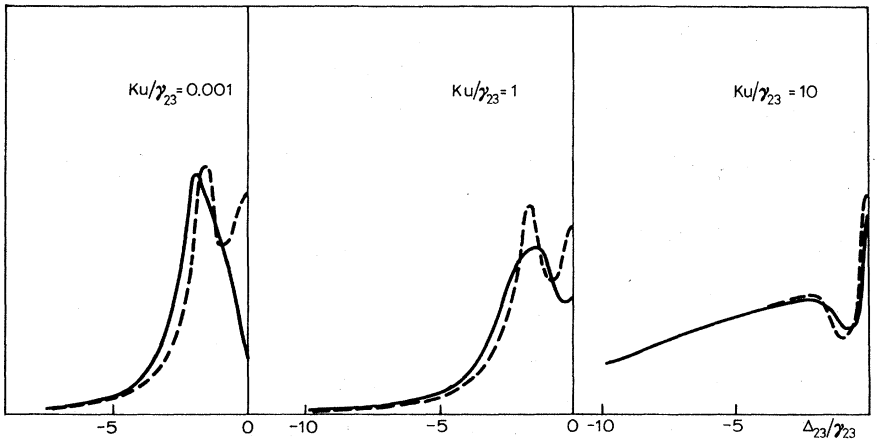


FIG. 9. This figure illustrates how the width $u$ of the Gaussian velocity distribution affects the shape of the absorption spectrum ($D_{23}^0$ term in arbitrary units). The accuracy of DFA (broken line, numerically integrated) improves as $Ku$ is increased. The spectra in the Doppler limit are shown in Fig. 3. Parameters: $\Delta_{21} = 0$, $\alpha^2 = 5\gamma_{23}^2$, and $\gamma_{13} = 0.1\gamma_{23}$.

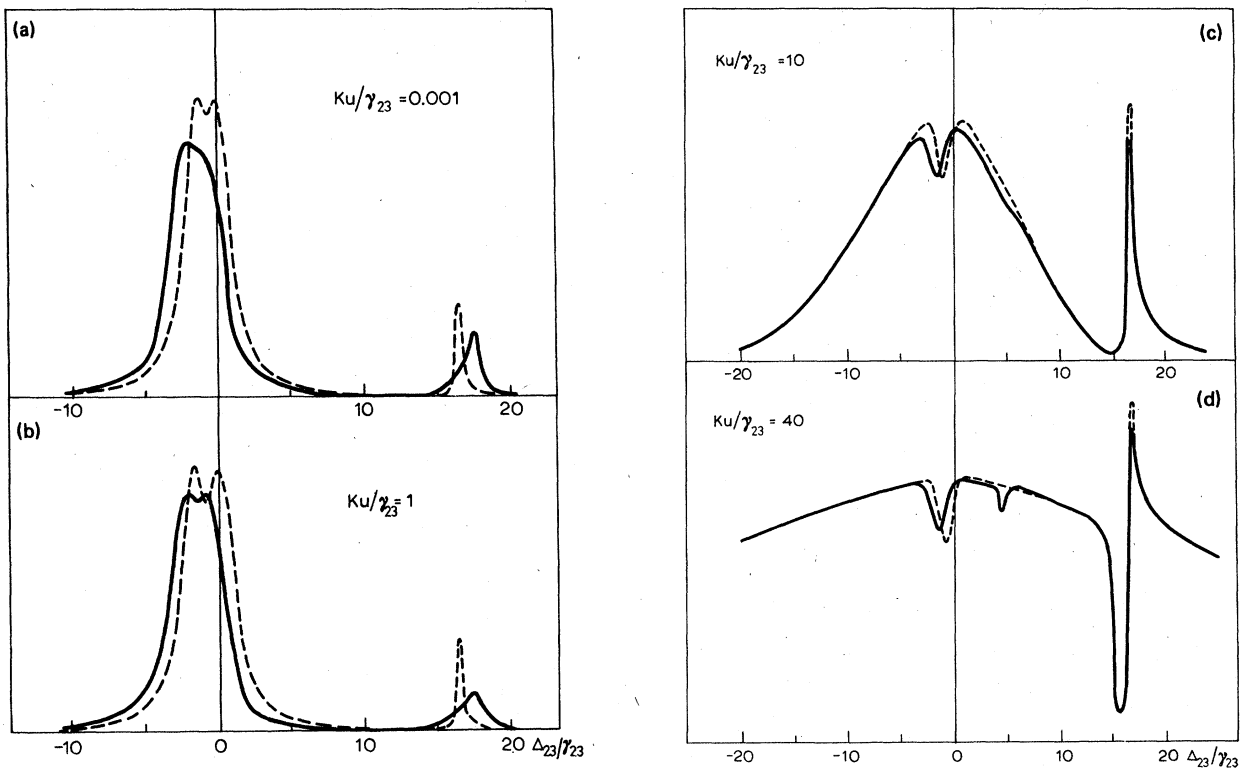


FIG. 10. The same as Fig. 9, but with $\Delta_{21}=15\gamma_{23}$ and $\alpha^2=50\gamma_{23}^2$. Note the absence of the maximum near $\Delta_{23}\approx 14\gamma_{23}$ which occurs in the Doppler limit (Fig. 5).

form the velocity averaging of (4.5) numerically instead of using (4.16)]. The main features of the spectra are correctly predicted by it; only small shifts and errors in the contrast of the dips appear in addition to the missing of some small scale structure. We have illustrated the quantitative accuracy of DFA in Fig. 11 in the special case $\Delta_{21}=\Delta_{23}=0$.

### E. $D_{21}^0$ term

If we have $D_{21}^0\neq 0$, the saturator induces average population changes and polarization $\rho_{21}^{(0)}$ to which the probe field reacts in addition to experiencing the dynamics of the strongly coupled transition. In the Doppler limit the velocity average of the $D_{21}^0$ term of the DFA can again be performed by contour integration (the lengthy expression is derived and briefly discussed in Appendix B).

According to (4.5) and the exact formulas (2.21) and (2.22) the following kind of effects can be distinguished.

(i) The Green's function $G(v)$ multiplying the source terms of (4.5) gives rise to a structure similar to the $D_{23}^0$ term. If the source terms vary slowly versus velocity (for instance, because of strong power broadening) they can be taken outside the velocity integral. As they also partly replace the role of the velocity selective Gaussian the results of Sec. IV D can be exploited.

(ii) The population-induced contribution, i.e., the second term in the curly brackets of (4.5), produces two power-broadened symmetric bumps at $\Delta_{23}\simeq\pm\Delta_{21}$ (Bennett holes). These are, however, strongly masked by the polarization-induced contribution and furthermore they are convoluted with the rather complicated function $G(v)$.

(iii) The polarization-induced contribution [third term in (4.5)] is mainly responsible for the asymmetry of the dips at $\Delta_{23}=\pm\Delta_{21}$ (recall the difference between forward and backward Raman-type signals). For a finite value of $Ku$ this contribution dominates the population-induced processes when the saturator is detuned outside the Doppler profile.

(iv) For simplicity all other effects are grouped into this category. These are typical high-intensity phenomena heavily mixed and only occasionally give rise to a clearly distinguishable peak in the strongly power-distorted probe spectrum.[25] They include corrections to $G$ and to the source terms (beyond DFA), and interference terms between them and those belonging to (i)–(iii).

Within the parameter range we have investigated the main features of the $D_{21}^0$ term are describable

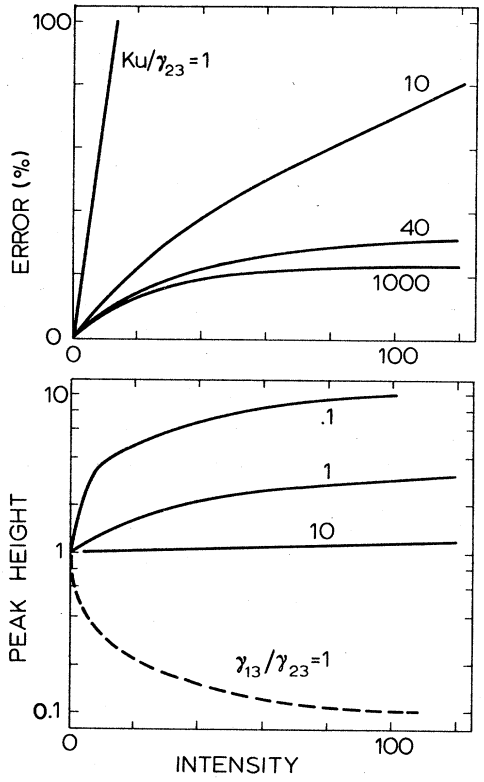


FIG. 11. The upper graph gives the relative error of DFA versus the saturator intensity $\alpha^2/\gamma_{23}^2$ for various Doppler widths ($\gamma_{13}=\gamma_{23}$) in exact resonance ($\Delta_{21}=\Delta_{23}=0$). In the lower part the peak height is shown for $Ku=1000_{\gamma 23}$ (solid lines) and $Ku=0$ (broken line). Note that in the homogeneous case the dimensionless saturation parameter is $\alpha^2/\gamma_{13}\gamma_{23}$ when only one curve is needed; this scaling holds only approximately for $Ku \neq 0$.

by the DFA which allows considerable simplifications in the computational work.

We do not aim at giving a full account of the parameter dependencies of the $D_{21}^0$ term. Figures 12 and 13 display the exact and DFA curves for various sets of relaxation parameters (note that changes in the decay rates also affect the degree of saturation). In the case $\Delta_{21}=0$ the $D_{21}^0$ term seems to be composed of a broad Lorentzian-like background and a superimposed narrower, more complicated peak. The former structure is due to population induced processes and the latter one to $G(v)$. This can be concluded by considering how the relaxation rates influence the spectra—increases in $\Gamma_i$ sharpens the background whereas the central peak depends mainly on the value of $\gamma_{13}$. As in the $D_{23}^0$ term, DFA slightly overestimates the contrast of the central sharp resonance. This can be explained by noting that $G(v)$ calculated with the DFA lacks the structure near $Kv=0$ (see Fig. 2), which in the $D_{21}^0$ term is weighed by the source terms (instead of the Gaussian). The overall agreement between the exact and DFA curves is, however, astonishingly good—according to a perturbation expansion of (2.22) DFA should be correct only to order $O(\alpha^2)$. The neglected terms probably contribute to the broad background and are heavily power broadened for large saturator intensities.

When the saturator is detuned ($\Delta_{21}\neq 0$) the resonant velocity groups move apart and interfere to a lesser extent. In Fig. 13 the saturation dips caused by the co- and counter-running TW components are seen in the gross shape of the spectrum—most clearly in the case $\Gamma_i=\gamma_{23}$ when excessive power broadening is absent. Near the point $\Delta_{23}=-\Delta_{21}$ DFA overestimates the signal. This is partly due to ignoring the $L_{13}(1)$ Lorentzian, and partly due to the fact that the REA does not account for splitting effects in the two-level system.[13] The discrepancy may be nonnegligible, but can easily be remedied by retaining $L_{13}(1)$ terms in the model. It is worth pointing out that the accuracy of the DFA improves as the population decay rates diminish: The reason for this is that the source terms are broadened and correspondingly the coherence terms ignored are more efficiently integrated away.

The spectrum near $\Delta_{23}=\Delta_{21}$ is more complicated than could be anticipated from a co-running TW configuration. For instance, in the case $\Gamma_i=\gamma_{ij}$ the TW model predicts a simple Lorentzian instead of the split resonance appearing in Fig. 13. The sharp structure is due to interference between the TW induced-polarization components and depends strongly on $\rho_{13}$ coherence. Some minor variation due to $G(v)$ is observable near $\Delta_{23}\simeq 0$, but there is very little evidence of the $\Delta_{21}/3$ dip which occurs in the $D_{23}^0$ term. The latter feature is expected because the dip disappears also from the $D_{23}^0$ term when $Ku$ is reduced. The overall agreement between the exact and DFA curves is very good (except the position $\Delta_{23}=-\Delta_{21}$). We do not present here a study on how finite Doppler widths influence the $D_{21}^0$ term. We just note that the effect of $Ku$ is probably less important than in the $D_{23}^0$ term because the velocity selection is already performed by the source terms.

### F. Role of various processes

In this chapter we briefly discuss how much the various processes contribute and study to what extent the SW spectra can be interpreted with the aid of the simpler TW models. As regards the $D_{23}^0$ term the structure seen in Figs. 6 and 7 is solely due to interference caused by the two saturator components: The TW formulas reproduce just a flat background in the Doppler limit. The

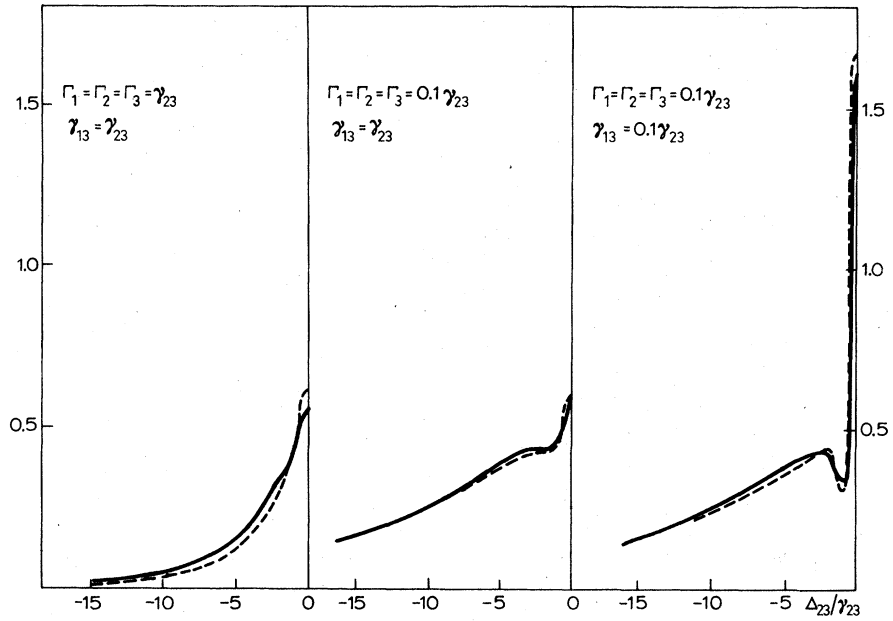


FIG. 12. The $D_{21}^0$ term (probe absorption in arbitrary units when the zero-field population difference of the probed transition is zero) for various sets of decay rates. The solid lines give the exact results; broken lines are DFA predictions. We have chosen $\Delta_{21}=0$, $\alpha^2=5\gamma_{23}^2$, and assumed the Doppler limit. The curves are symmetric with respect to $\Delta_{23}$.

situation does not change if for $G(v)$ we use the independent-field approximation $G(v)=1/a(0)$ [see (2.25)]. When the Doppler width is reduced some structure appears. In the extreme case $Ku\to 0$ we find the following from (2.25) by neglecting cross effects ($S_+=S_-=0$):

$$\langle\rho_{23}\rangle=-i\alpha_2 D_{23}^0 L_{23}(1+\tfrac{1}{2}\alpha^2 L_{13}L_{23})^{-1}, \qquad (4.18)$$

which is correct to order $O(\alpha^2)$ only,[11,20] as expected.

In the simple case when we have $\Gamma_{21}=\Gamma_{23}=0$ and $\gamma_{ij}=\frac{1}{2}(\Gamma_i+\Gamma_j)$, the superposition of TW results suggests that the $D_{21}^0$ term should comprise two Lorentzians having the widths

$$\tilde{\gamma}_+=\tfrac{1}{2}[\Gamma_3+\Gamma_1(1+\alpha^2/\Gamma_1\Gamma_2)^{1/2}], \qquad (4.19)$$

$$\tilde{\gamma}_-=\tfrac{1}{2}[\Gamma_3+(\Gamma_1+2\Gamma_2)(1+\alpha^2/\Gamma_1\Gamma_2)^{1/2}], \qquad (4.20)$$

and being located at $\Delta_{23}=\Delta_{21}$ and $\Delta_{23}=-\Delta_{21}$, respectively. Both Lorentzians are too highly power broadened to explain the sharp structure occurring in Fig. 13 which, therefore, must be due to interference effects. (Note that the above assumption of relaxation rates is not essential.)

A measure of the importance of interference effects in a SW field is obtained by comparing (4.19) and (4.20) or the power-broadened width

$$\Gamma=\gamma_{21}[1+\tfrac{1}{2}\alpha^2(\Gamma_1+\Gamma_2-\Gamma_{21})/\gamma_{21}\Gamma_1\Gamma_2]^{1/2} \qquad (4.21)$$

[for $\Delta_{21}=0$ replace $\alpha^2$ by $2\alpha^2$; cf. (B3) and (B10)] to the saturator detuning $\Delta_{21}$. $\Gamma$ describes the width of the source terms in (4.5). The magnitude of the convergence factor $\xi(m)$, Eq. (3.1), determines the strength of interaction between $\alpha_+^2$ and $\alpha_-^2$ within the Green's function $G$; when using the DFA we can readily apply the dimensionless saturation parameter $\alpha^2/\gamma_{13}\gamma_{23}$ for $\Delta_{21}=0$ or $\alpha^2/\gamma|\Delta_{21}|$ for a detuned situation.

We want to emphasize that arguments concerning the resonant velocity groups are strictly valid for the population-induced processes only. Off-resonant groups contribute considerably to the polarization-induced processes and can partly cancel the step-wise terms—for instance, in (4.19) there is no trace of the width $(\gamma_{23}+\Gamma)$ that would result from the convolution between $L_{23}(0)$ and the Bennett holes in $\rho_{22}^{(0)}$. The relative importance of population- and polarization-induced contributions depends strongly on the relaxation scheme in addition to the laser detunings. In resonance the ratio of their magnitudes is roughly measured by the quantity $\Gamma_2/\gamma_{13}$—a large value of $\Gamma_2$ implies that population processes are heavily suppressed.

According to (4.21) the transition $1\leftrightarrow 2$ is heavily power broadened if the population decay rates are small. Then the dominant structure in the $D_{21}^0$ term arises from $G(v)$—the situation is the same as in the $D_{23}^0$ term: The excitation of the $1\leftrightarrow 2$ system is only poorly velocity selective. The similarity between the dip regions in Figs. 7 and 13 clearly results from the absence of atoms satisfying the resonance conditions of $G(v)$ [cf. (4.13)].

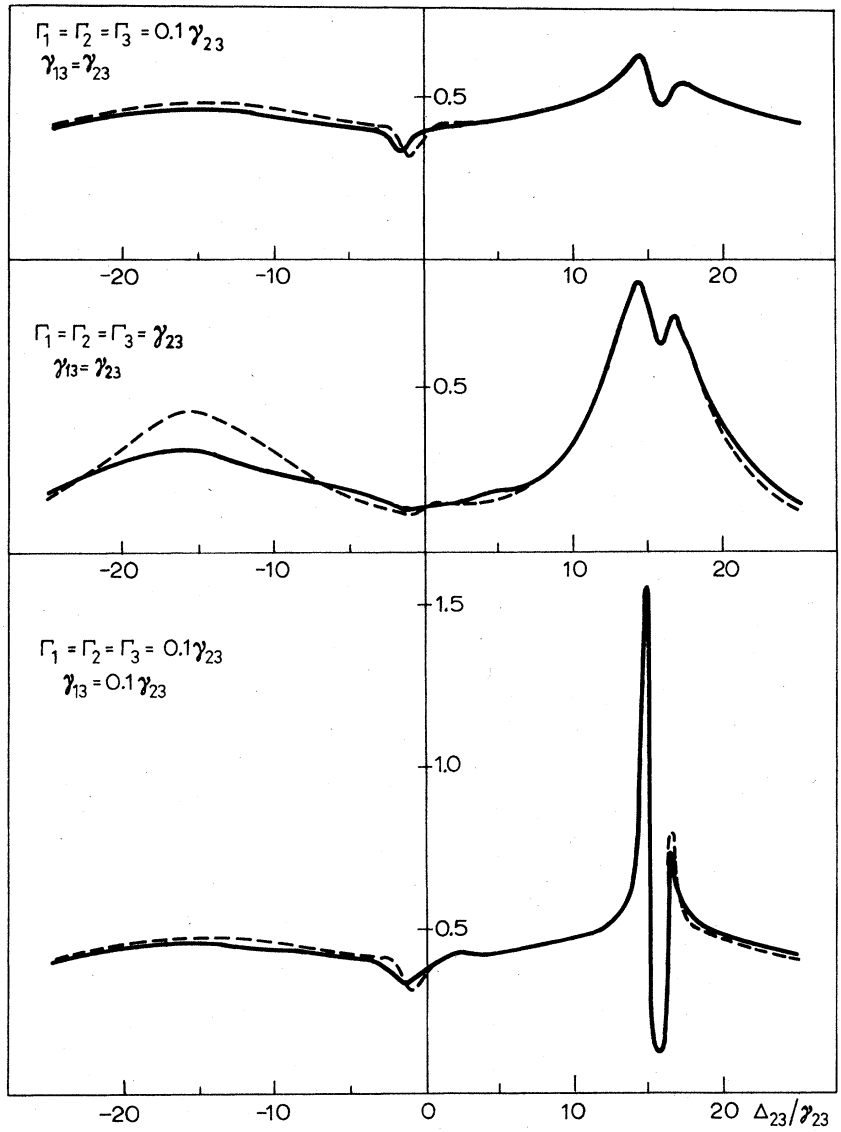


FIG. 13. The same as Fig. 12, but with $\Delta_{21} = 15\gamma_{23}$ and $\alpha^2 = 50\gamma_{23}^2$. Note how the accuracy of DFA near $\Delta_{23} = -\Delta_{21}$ improves as $\Gamma_{1,2}$ is decreased; the magnitude of $\gamma_{13}$ affects the behavior near $\Delta_{23} = \Delta_{21}$ mainly.

Small differences between the $D_{23}^0$ and $D_{21}^0$ terms are explainable by effects due to the finite width $\Gamma$ of the excited velocity distribution.

In Figs. 14 and 15 we have separated the various contributions to the overall $D_{21}^0$ term. The graphs are based on the exact formula (2.22) and the division is such that the population term includes the $D_{23}(0)$ part of $d(0)$ (multiplied by $G$), the polarization term the rest of $d(0)$ [see (2.21)], and the sum terms are all grouped together. The IFA model of Feldman and Feld[9] is obtained by replacing the Green's function $G$ by a Lorentzian in the population term. As seen from the figures it is unable to reproduce the sharp structure, in contrast to DFA (cf. Figs. 12 and 13), but accounts satisfactorily for the broader background. The population-induced processes are clearly causing the background. This is further manifested in Fig. 16 where an increase in $\Gamma_2$ destroys the background. The rapid variations in the population term due to $\langle G \rangle$ vanish because of velocity selection but remain in the polarization-induced contribution which is restricted to a rather narrow region in the vicinity of $\Delta_{23} = \Delta_{21}$. Away from this resonance we expect the zero-area rule to be valid for the coherence processes. The small residual absorption is a nonresonant correction. The remaining sum term, part of which is included in the DFA,

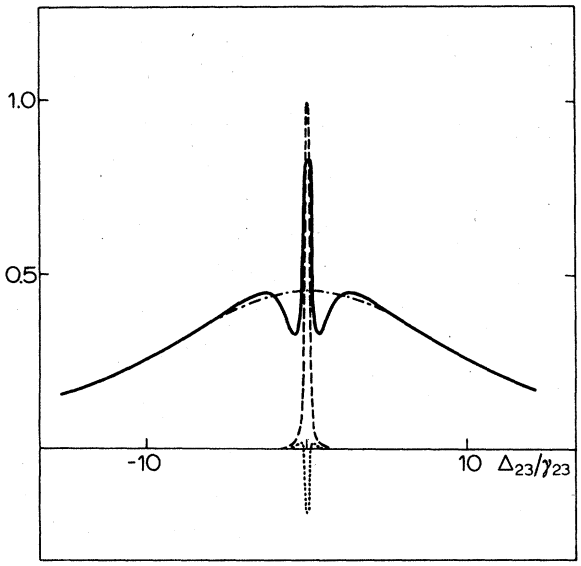


FIG. 14. Various contributions to the $D_{21}^0$ term in the Doppler limit (for total spectrum see Fig. 12): The solid line gives the population term, the broken line gives the polarization term, and the dotted line gives the rest; the dash-dotted curve is the independent-field approximation of Ref. 9. Parameters are $\Delta_{21}=0$, $\alpha^2=5\gamma_{23}^2$, $\Gamma_1=\Gamma_2=\Gamma_3=\gamma_{13}=0.1\gamma_{23}$.

has a similar shape as the polarization term and does not add any remarkable new features. We can conclude that a simple superposition of TW results explains the broad background of the $D_{21}^0$ term. The regions of strongly reduced absorption, as also the sharp peaks appearing in the vicinity of $\Delta_{23}=\Delta_{21}$, are entirely due to interference effects.

## V. SUMMARY AND DISCUSSION

In this paper we have solved the three-level problem where one transition is saturated by an arbitrary intense standing wave and an adjacent transition is probed by a weak field. The model system includes a rather general relaxation scheme and allows unequal amplitudes for the TW components of the saturator which extend the validity of previous theories and facilitate the identification of various contributions.

The general solution expressed in terms of continued fractions is rather cumbersome and therefore we have derived the DFA with which the parameter analysis is expediently performed. In addition to the assumptions ordinarily made in the steady-state three-level models (RWA, degeneracy, phenomenological collision rates, etc.), DFA also

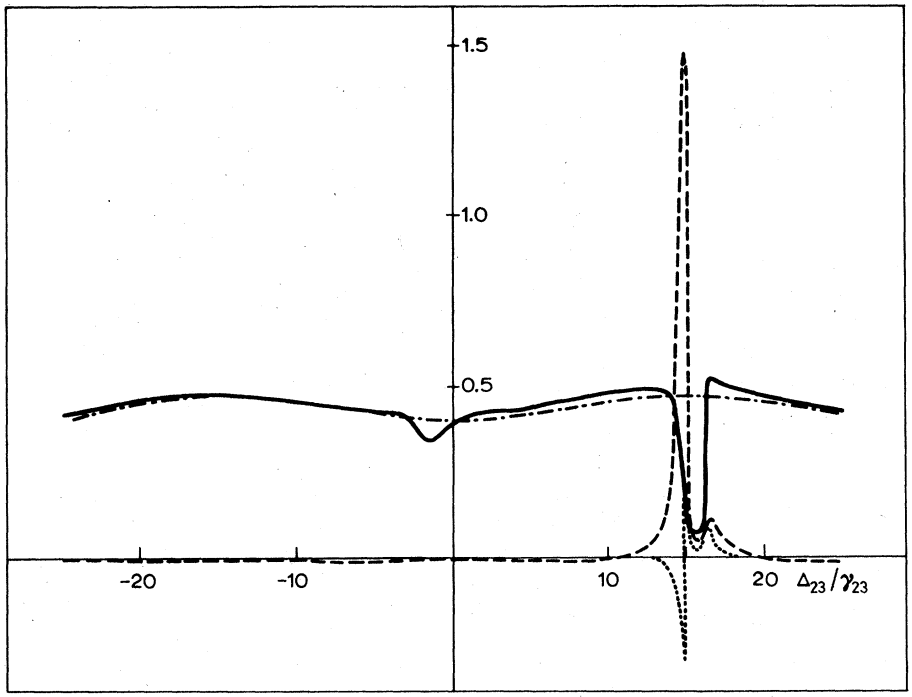


FIG. 15. The same as Fig. 14, but with $\Delta_{21}=15\gamma_{23}$ and $\alpha^2=50\gamma_{23}^2$ and the total response given in Fig. 13 (bottom spectrum).

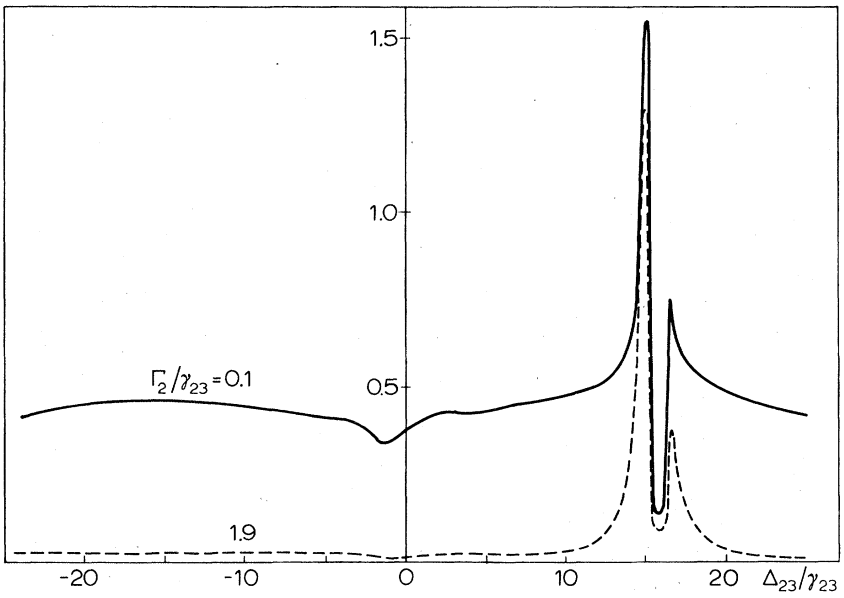


FIG. 16. This figure manifests how the population induced contribution in the $D_{21}^0$ term vanishes as $\Gamma_2$ is increased from $0.1\gamma_{23}$ to $1.9\gamma_{23}$. Other parameters as in Fig. 15. Note the reduction of the height of the peak at $\Delta_{23} \simeq 14\gamma_{23}$ which is partly explainable by the velocity cut-off arguments.

presumes that $K_1 \simeq K_2$ which allows us to neglect all other $\rho_{13}$ coherences except the one free of Doppler effects. The condition $|K_1 - K_2| u < \gamma_{13}$ may be quite restrictive. Solutions which relax this are, however, easily obtained by truncating the general formula more symmetrically—e.g., by retaining the Lorentzian $L_{13}(1)$, too. The validity of DFA has been verified by a numerical comparison to the exact results in a relatively broad parameter range.

We have split the response into two according to zero-field population differences. The $D_{23}^0$ term reflects the dynamics of the strongly coupled system $1 \rightarrow 2$. In the $D_{21}^0$ term average population and polarization changes (which themselves are also distinquishable) introduce additional features. Although DFA may be largely erroneous for some velocity groups the Doppler average of both contributions is quite accurate leaving out only some minor structure—higher-order coherences are dephased (zero-area property). We have also demonstrated that important SW modifications occur in the response as compared to simple TW superposition models.

The dominant structure of the probe response appears near the detunings $\Delta_{23} = 0$, $\Delta_{21}$, and $\frac{1}{2}\Delta_{21} \pm \frac{1}{2}(\Delta_{21}^2 + 2\alpha^2)^{1/2}$. The actual shapes of the resonances are shown to be sensitive to the width of the velocity distribution which preferentially samples the contribution of slow atoms (in time space this means incomplete Doppler dephasing). The qualitative differences between the homogeneous and inhomogeneous spectra reveal the weakness of the argument that zero-velocity atoms give rise to the sharp structures—in fact, off-resonant atoms are equally important.

The ac-Stark effect which is clearly manifested in $G(v)$ for a TW saturator is much more obscure in the SW case. This is, of course, due to the fact that a moving atom sees a periodically modulated field amplitude and its simple sinusoidal Rabi flipping is replaced by a more complicated time dependence. The splitting taking place in the velocity-averaged response can be explained by the lack of resonant atoms in TW configurations. The same argument seems to apply to the SW case, too. A physical explanation to this would certainly be worth further studies.

The model system considered has a rather complicated saturation behavior. Ordering action is measured by the flipping parameters $\alpha_\pm^2$; dephasing appears because of $\Delta_{21}$, $\Delta_{23}$, and $Kv$ (note the resonant enhancement); real relaxation phenomena are represented by the decay rates $\Gamma_i$ and $\gamma_{ij}$. A comparison between $\alpha$ and the dephasing times ($\Delta^{-1}$ or $\gamma^{-1}$) reproduces the saturation parameters mentioned in Sec. IV. This kind of view emphasizes the role of the dynamics even though the main intensity dependence of the steady-state spectra may be disguised in power broadening.

The relative magnitude of the relaxation rates

strongly affects the shape of the spectra by stressing certain physical processes. They also determine which approximate model should be preferred. The IFA of Ref. 9 is expected to hold in a laserlike transition where the lower levels decay rapidly ($\gamma_{13} \gg \gamma_{23}$); narrow resonances, on the other hand, are found in the DFA region ($\gamma_{13} \ll \gamma_{23}$).

Finally we want to mention a few topics worth future work. First of all the case $K_1 \neq K_2$ is of considerable interest and can be treated with the results of Sec. II. Analogous approximations such as DFA are quite easily found. We have assumed a weak probe which does not cause any saturation. In experiments this may be impracticable when the theory should be extended. Higher-order perturbation expansion in terms of $\alpha_2$ can be performed, but then the mathematics becomes extremely tedious. It might be, therefore, advisable to do the simplifying approximations already in Eqs. (2.1)–(2.6). Also the probe may be a standing wave, e.g., a laser mode near threshold. Then there appears coupling between the TW components of the probe[26] which can give rise to new interesting phenomena. As regards the basic physics it would be valuable to study the dynamics of the considered configuration in more detail in order to get a better understanding of the mechanism causing the disappearance of resonant atoms.

ACKNOWLEDGMENTS

The authors are grateful for valuable discussions to Professor P. Berman, Professor S. Stenholm, and Professor P. Toschek. One of us (E.K.) also wishes to thank the Emil Aaltonen Foundation for financial support.

## APPENDIX A: CONTINUED FRACTION SOLUTION

Inserting (2.8)–(2.11) into (2.1)–(2.6) yields the recurrence relations

$$L_{21}^{-1}(m)\rho_{21}(m) = -i\alpha_+ D_{21}(m-1) - i\alpha_- D_{21}(m+1) + i\alpha_2 \rho_{13}^*(-m)\,, \tag{A1}$$

$$L_{23}^{-1}(m)\rho_{23}(m) = -i\alpha_2 D_{23}(m) + i\alpha_+ \rho_{13}(m-1) + i\alpha_- \rho_{13}(m+1)\,, \tag{A2}$$

$$L_{13}^{-1}(m)\rho_{13}(m) = -i\alpha_2 \rho_{21}^*(-m) + i\alpha_+^* \rho_{23}(m+1) + i\alpha_-^* \rho_{23}(m-1)\,, \tag{A3}$$

$$(\Gamma_1 + imK_1 v)\rho_{11}(m) = \Gamma_1 n_1^0(m) + \Gamma_{21}\rho_{22}(m) + \kappa_{31}\rho_{33}(m) - W_{21}(m)\,, \tag{A4}$$

$$(\Gamma_2 + imK_1 v)\rho_{22}(m) = \Gamma_2 n_2^0(m) + W_{21}(m) - W_{23}(m)\,, \tag{A5}$$

$$(\Gamma_3 + imK_1 v)\rho_{33}(m) = \Gamma_3 n_3^0(m) + \Gamma_{23}\rho_{22}(m) + \kappa_{13}\rho_{11}(m) - W_{23}(m)\,, \tag{A6}$$

where

$$D_{ij}(m) = \rho_{ii}(m) - \rho_{jj}(m)\,, \tag{A7}$$

$$W_{21}(m) = -i[\alpha_+^* \rho_{21}(m+1) + \alpha_-^* \rho_{21}(m-1) - \alpha_+ \rho_{21}^*(1-m) - \alpha_- \rho_{21}^*(-1-m)]\,, \tag{A8}$$

$$W_{23}(m) = -i[\alpha_2^* \rho_{23}(m) + \alpha_2 \rho_{23}(-m)]\,, \tag{A9}$$

and the Lorentzians $L_{ij}(m)$ are defined by (2.14)–(2.16) and $\Gamma_i n_i^0(m)$ is the Fourier component of the incoherent pumping rate—in the following we take $n_i^0(m) = n_i^0 \delta_{m,0}$. A solution of (A1)–(A6) valid for an arbitrary $\alpha_2$ might be found by exploiting matrix techniques for the recurrence relations.[10,12] Instead of this we use perturbation theory keeping $\alpha_2$ as the small parameter.

### Zeroth-order solution

This case has been discussed before[12] and we just list the equations needed to evaluate $\rho_{ij}^{(0)}$. For $D_{21}(m)$ we have

$$D_{21}(m) = R_+(m) R_+(m-2) \cdots R_+(2) D_{21}(0) \quad (m > 0) \tag{A10}$$

$$D_{21}(m) = R_-(m) R_-(m+2) \cdots R_-(-2) D_{21}(0) \quad (m < 0) \tag{A11}$$

$$D_{21}(0) = D_{21}^0 [A(0) + B(0) R_+(2) + C(0) R_-(-2)]^{-1}\,, \tag{A12}$$

where the continued fractions $R_\pm$ are defined by

$$R_+(m) = -C(m)[A(m) + B(m) R_+(m+2)]^{-1}\,, \tag{A13}$$

$$R_-(m) = -B(m)[A(m) + C(m) R_-(m-2)]^{-1}\,, \tag{A14}$$

$$A(m) = 1 + g(m)\{\alpha_+^2 [L_{21}(m+1) + L_{21}^*(1-m)] + \alpha_-^2 [L_{21}(m-1) + L_{21}^*(-1-m)]\}\,, \tag{A15}$$

$$B(m) = \alpha_- \alpha_+^* g(m)[L_{21}(m+1) + L_{21}^*(-1-m)]\,, \tag{A16}$$

$$C(m) = \alpha_-^* \alpha_+ g(m)[L_{21}(m-1) + L_{21}^*(1-m)]\,, \tag{A17}$$

$$g(m)=\frac{1}{\Gamma_2+imK_1v}\times\left(1+\frac{(\Gamma_3+imK_1v)(\Gamma_2-\Gamma_{21}+imK_1v)-\kappa_{31}\Gamma_{23}}{(\Gamma_1+imK_1v)(\Gamma_3+imK_1v)-\kappa_{13}\kappa_{31}}\right). \tag{A18}$$

$D_{21}^0$ is the zero-field population difference [put $W_{21}=W_{23}=0$ in (A4)–(A6)]. The off-diagonal component $\rho_{21}^{(0)}$ is given by

$$\rho_{21}^{(0)}(m)=-iL_{21}(m)[\alpha_+D_{21}(m-1)+\alpha_-D_{21}(m+1)]. \tag{A19}$$

The populations $\rho_{ii}^{(0)}(m)$ are obtained by solving (A4)–(A6) in terms of $W_{21}(m)$ which is related to $D_{21}(m)$ by

$$D_{21}(m)=D_{21}^0\delta_{m,0}+g(m)W_{21}(m). \tag{A20}$$

[Note that $W_{23}(m)=0$ in the zeroth order.] For the "decoupled" transition $2\leftrightarrow 3$ we have $\rho_{23}^{(0)}=0$, $\rho_{13}^{(0)}=0$, and the population difference

$$D_{23}(m)=D_{23}^0\delta_{m,0}+f(m)[D_{21}(m)-D_{21}^0\delta_{m,0}], \tag{A21}$$

$$f(m)=\frac{(\Gamma_1+imK_1v)(\Gamma_3+imK_1v-\Gamma_{23})+\kappa_{13}(\Gamma_2+imK_1v-\Gamma_{21}-\kappa_{31})}{(\Gamma_3+imK_1v)(\Gamma_1+\Gamma_2-\Gamma_{21}+2imK_1v)-\kappa_{31}(\kappa_{13}+\Gamma_{23})}, \tag{A22}$$

with the aid of $D_{21}(m)$ we can evaluate all zeroth-order terms $\rho_{ij}^{(0)}(m)$.

### First-order perturbation

The level populations and $\rho_{21}(m)$ do not acquire any first-order corrections. The nonvanishing components $\rho_{23}(m)$ and $\rho_{13}(m)$ (we drop the order index) are determined by (2.12) and (2.13) readily obtained from (A2) and (A3). The inhomogeneous difference equation (2.17) can be solved with Green functions $G(m,m')$ defined by

$$a(m)G(m,m')+b(m)G(m+2,m')+c(m)G(m-2,m')=\delta_{m,m'}. \tag{A23}$$

The complete solution reads then

$$\rho_{23}(m)=\sum_{m'}G(m,m')d(m'). \tag{A24}$$

Equation (A23) has exactly the same form as the one derived for $D_{21}(m)$ in the zeroth order, and we find

$$G(m,m')=s_+(m)s_+(m-2)\cdots s_+(m'+2)G(m',m') \quad (m>m') \tag{A25}$$

$$G(m,m')=s_-(m)s_-(m+2)\cdots s_-(m'-2)G(m',m') \quad (m<m') \tag{A26}$$

$$G(m,m')=[a(m')+b(m')s_+(m'+2)+c(m')s_-(m'-2)]^{-1}, \tag{A27}$$

where the continued fractions are defined by

$$s_+(m)=-c(m)[a(m)+b(m)s_+(m+2)]^{-1}, \tag{A28}$$

$$s_-(m)=-b(m)[a(m)+c(m)s_-(m-2)]^{-1}. \tag{A29}$$

Next we relate $G(m',m')$ to $G=G(0,0)$. From (A27) we obtain with the aid of (A28) and (A29):

$$G(m',m')=\frac{s_+(m')b(m'-2)}{c(m')s_-(m'-2)}G(m'-2,m'-2)=\frac{s_-(m')c(m'+2)}{b(m')s_+(m'+2)}G(m'+2,m'+2). \tag{A30}$$

Inserting $G(m',m')$ expressed in terms of $G(0,0)$ into (A24) and introducing the transformation

$$S_-(m)=\frac{c(m+2)}{b(m)}s_-(m), \tag{A31}$$

$$S_+(m)=\frac{b(m-2)}{c(m)}s_+(m), \tag{A32}$$

we get the final result (2.22) given in the text. The source term $d(m)$, Eq. (2.21), is according to (A19) and (A21):

$$d(m)=i\alpha_2\{D_{23}^0\delta_{m,0}+f(m)[D_{21}(m)-D_{21}^0\delta_{m,0}]-L_{13}(m-1)L_{21}^*(1-m)[\alpha_+^2D_{21}(m)+\alpha_+\alpha_-^*D_{21}(m-2)]-L_{13}(m+1)L_{21}^*(-1-m)[\alpha_-\alpha_2^*D_{21}(m+2)+\alpha_-^2D_{21}(m)]\}. \tag{A33}$$

One can verify that $\rho_{23}(0)$ does not depend on the relative phase between $\alpha_+$ and $\alpha_-$. Note also that all components $\rho_{23}(m)$ are obtained by (A24), though we need only $\rho_{23}(0)$.

## APPENDIX B: DFA

Insertion of (4.6) and (4.7) into (4.5) yields

$$\rho_{23}=-i\alpha_2D_{23}^0G+i\alpha_2D_{21}^0G\frac{1}{A(0)}\left(f[A(0)-1]+\frac{\alpha_+^2L_{13}L_{21}^*(1)}{1+\alpha_-^2L_{13}L_{23}(-2)}\right), \tag{B1}$$

where $A(0)$ and $f=f(0)$ are defined by (A15) and (A22), respectively. For $K_1=K_2=K$ and $\alpha_+^2=\alpha_-^2=\frac{1}{4}\alpha^2$ the poles of $G$ are given by (4.12):

$$Kv=\pm x=\pm iL_{23}^{-1}(1+\tfrac{1}{2}\alpha^2 L_{13}L_{23})^{1/2} \tag{B2}$$

and the zeroes of $A(0)$ by

$$Kv=\pm y_\pm=\pm[\Delta_{21}^2-\gamma_{21}^2-\tfrac{1}{2}\gamma_{21}g\alpha^2\pm i(4\gamma_{21}^2\Delta_{21}^2+2\gamma_{21}\alpha^2 g\Delta_{21}^2-\tfrac{1}{4}\gamma_{21}^2\alpha^4 g^2)^{1/2}]^{1/2}, \tag{B3}$$

where $g=g(0)$, see Eq. (A18). We make the sign convention $\mathrm{Im}(x)>0$ and $\mathrm{Im}(y_\pm)>0$. The velocity average of (B1) can be performed with the aid of the plasma dispersion function (for details see, e.g., Ref. 23), or in the Doppler limit ($|x|, |y_\pm| \ll Ku$) by a simple contour integration, which case is assumed in the following.

For the $D_{23}^0$ term we get the result (4.16) which can be written also as

$$\langle\rho_{23}\rangle=\frac{i\alpha_2\pi^{1/2}}{Ku}D_{23}^0\left[1+\frac{\alpha^2}{8}\left(L_{13}L_{23}-\frac{1}{L_{23}^{-1}L_{13}^{-1}+\alpha^2/2}\right)\right]^{1/2}. \tag{B4}$$

In the limit $\alpha^2\to 0$ we have

$$\langle\rho_{23}\rangle=\frac{i\alpha_2\pi^{1/2}}{Ku}D_{23}^0(1+\tfrac{1}{32}\alpha^4L_{13}^2L_{23}^2-\tfrac{1}{64}\alpha^6L_{13}^3L_{23}^3+\cdots). \tag{B5}$$

The two terms in (B4) producing resonance structure at $\Delta_{23}=0$ or $\Delta_{21}$ and at $\Delta_{23}=\frac{1}{2}\Delta_{21}\pm\frac{1}{2}(\Delta_{21}^2+2\alpha^2)^{1/2}$ become separated as $\alpha^2$ increases. Then we obtain the approximate line shape

$$\langle\rho_{23}\rangle=\frac{i\alpha_2\pi^{1/2}}{Ku}D_{23}^0(\alpha^2L_{13}L_{23}/8)^{1/2} \tag{B6}$$

for the case $\alpha^2|L_{13}L_{23}|\gg 1$. This is a pure Lorentzian when $\Delta_{21}=0$ and $\gamma_{13}=\gamma_{23}$; for $\Delta_{21}\neq 0$ the absorption follows the shape $\mathrm{Re}[(\Delta_{23}-i\gamma_{23})^{-1/2}]$ near $\Delta_{23}=0$ and $\mathrm{Re}[(\Delta_{23}-\Delta_{21}-i\gamma_{13})^{-1/2}]$ near $\Delta_{23}=\Delta_{21}$. For the side peaks we similarly derive, e.g.,

$$\langle\rho_{23}\rangle\simeq\frac{i\alpha_2\pi^{1/2}}{Ku}D_{23}^0\left(\frac{\alpha\sqrt{2}}{16}\right)^{1/2}\times[(\Delta_{23}-\alpha/\sqrt{2})-\tfrac{1}{2}i(\gamma_{13}+\gamma_{23})]^{-1/2} \tag{B7}$$

for $|\Delta_{23}-(\alpha^2/2)^{1/2}|$, $\gamma_{13}$, $\gamma_{23}\ll(\alpha^2/2)^{1/2}$, and $\Delta_{21}=0$. The asymmetry of $\mathrm{Im}(\langle\rho_{23}\rangle)$ is easily seen by putting $\gamma_{13}=\gamma_{23}=0$.

The $D_{21}^0$ term is given by ($\kappa_{13}=\kappa_{31}=0$)

$$\begin{aligned}\langle\rho_{23}\rangle=&-\frac{\alpha_2\alpha^2\pi^{1/2}}{Ku}D_{21}^0[(x+y_+)(x+y_-)(y_++y_-)]^{-1}\\&\times\Big\{\gamma_{21}\frac{\Gamma_3-\Gamma_{23}}{\Gamma_2\Gamma_3}(\gamma_{23}+i\Delta_{23}+\tfrac{1}{4}\alpha^2L_{13})\left(\frac{\gamma_{21}^2+\Delta_{21}^2}{xy_+y_-}(x+y_++y_-)-1\right)\\&+\tfrac{1}{4}L_{13}\Big[xy_++xy_-+y_+y_--(\gamma_{21}+i\Delta_{21})^2\\&+(\gamma_{21}-i\Delta_{21})(\gamma_{23}+i\Delta_{23})\left(\frac{(\gamma_{21}+i\Delta_{21})^2}{xy_+y_-}(x+y_++y_-)-1\right)\Big]\Big\}.\end{aligned} \tag{B8}$$

By a manipulation of the residues of (B1) we have removed from (B8) the apparent singularities like $(x-y_\pm)$. The advantage of the complicated expression (B8) is that the velocity averaging is exact.

For a resonant saturator ($\Delta_{21}=0$) we have

$$y_-=i\gamma_{21}, \tag{B9}$$

$$y_+=i\Gamma=i(\gamma_{21}^2+\gamma_{21}g\alpha^2)^{1/2}, \tag{B10}$$

$$x=iL_{23}^{-1}\zeta=iL_{23}^{-1}(1+\tfrac{1}{2}\alpha^2L_{13}L_{23})^{1/2}, \tag{B11}$$

which inserted into (B8) yield

$$\langle\rho_{23}\rangle=\frac{i\alpha_2\alpha^2\pi^{1/2}}{4Ku}\frac{D_{21}^0}{\Gamma+\zeta L_{23}^{-1}}\times\left[L_{13}\left(\Gamma+\frac{\gamma_{21}}{\zeta}\right)+4\frac{\gamma_{21}}{\zeta}\frac{\Gamma_3-\Gamma_{23}}{\Gamma_2\Gamma_3}(1+\tfrac{1}{4}\alpha^2L_{13}L_{23})\right]. \tag{B12}$$

The limit $L_{13}\to 0$ reproduces the familiar REA expression. Resonance structure appears near $\Delta_{23}=0$ ($|L_{13}|$ and $|L_{23}|$ large) and near $|\Delta_{23}|=(\alpha^2/2)^{1/2}$ ($|\zeta^{-1}|$ large). The central structure is described by the Lorentzian

$$\langle\rho_{23}\rangle=\frac{i\alpha_2\alpha^2\pi^{1/2}}{4Ku}D_{21}^0\frac{\Gamma}{\Gamma+(\alpha^2/2)^{1/2}}\times\left(1+\gamma_{21}\frac{\Gamma_3-\Gamma_{23}}{\Gamma_2\Gamma_3}\frac{(2\alpha^2)^{1/2}}{\Gamma}\right)L_{13} \tag{B13}$$

provided that we have $\alpha^2|L_{13}L_{23}|\gg 1$ and $\gamma_{13}=\gamma_{23}$. Note that the peak height increases as $\alpha^2$. In the limit $|\Delta_{21}|\to\infty$, Eq. (B8) correctly predicts the expected TW result near $\Delta_{23}=\Delta_{21}$, but gives only a REA formula near $\Delta_{23}=-\Delta_{21}$ (counter-running case). Expansions of (B8) which take into account the interference between the TW components (especially near $\Delta_{23}=\Delta_{21}$) are rather complicated and are not reproduced here.

[1]For a review see, e.g., V. S. Letokhov and V. P. Chebotayev, *Nonlinear Laser Spectroscopy* (Springer, Heidelberg, (1977).
[2]R. Keil and P. E. Toschek, Kvant. Elektron. (Moscow) 5, 1664 (1978) [Sov. J. Quantum Electron. 8, 949 (1978)].
[3]J. Reid and T. Oka, Phys. Rev. Lett. 38, 67 (1977).
[4]J. P. Woerdman and M. F. H. Schuurmans, Opt. Commun. 21, 243 (1977).
[5]M. Himbert, S. Reynaud, J. DuPont-Roc, and C. Cohen-Tannoudji, Opt. Commun. 30, 184 (1979).
[6]For reviews see, e.g., K. Shimoda, in *Laser Spectroscopy of Atoms and Molecules*, edited by H. Walther, (Springer, Heidelberg, 1976) Vol. 2, pp. 197–252; T. Oka, in *Frontiers in Laser Spectroscopy*, edited by R. Balian, S. Haroche, and S. Liberman (North-Holland, Amsterdam, 1977), Vol. 2, pp. 530–569.
[7]F. Najmbadi, M. Sargent III, and F. A. Hopf, Phys. Rev. A 12, 1553 (1975).
[8]W. Neuhauser and P. E. Toschek, Opt. Commun. 11, 331 (1974).
[9]B. J. Feldman and M. S. Feld, Phys. Rev. A 5, 899 (1972).
[10]A. H. Paxton and P. W. Milonni, Opt. Commun. 34, 111 (1980).
[11]E. Kyrölä and R. Salomaa, Appl. Phys. 20, 339 (1979).
[12]S. Stenholm and W. E. Lamb, Jr., Phys. Rev. 181, 618 (1969); S. Haroche and F. Hartmann, Phys. Rev. A 6, 1280 (1972); J. H. Shirley, *ibid.* 8, 347 (1973); R. Salomaa and S. Stenholm, *ibid.* 8, 2695 (1973); J. B. Hambenne and M. Sargent III, *ibid.* 13, 784 (1976); A. Bambini, *ibid.* 14, 1479 (1976); J. Ziegler and P. R. Berman, *ibid.* 16, 681 (1977); K. Kuroda, *ibid.* 19, 231 (1979).
[13]E. Kyröla, Report No. HU-TFT-80-3, Physica Scripta (in press).
[14]V. P. Chebotayev and B. Ya. Dubetsky, Appl. Phys. 18, 217 (1979); B. Ya. Dubetsky, *ibid.* 19, 225 (1979).
[15]See, e.g., M. S. Feld and A. Javan, Phys. Rev. 177, 540 (1969) and T. Ya Popova, A. K. Popov, S. G. Rautian, and R. I. Sokolovskii, Zh. Eksp. Teor. Fiz. 57, 850 (1969) [Sov. Phys.–JETP 30, 466 (1970)].
[16]For a TW probe the component $\exp[i(2K_1-K_2)z]$, which in the case $K_1 \simeq K_2$ reduces to $\exp(iK_2z)$, is excluded when performing the RWA. When a SW probe is used there may appear coupling between the probe components (see Ref. 26).
[17]M. Sargent III, M. O. Scully, and W. E. Lamb, Jr., *Laser Physics*, (Addison-Wesley, Reading, Mass., 1974), Chaps. 7 and 8.
[18]The simpler form of the continued fractions in Ref. 9 is entirely due to the assumption $|\alpha_+| = |\alpha_-|$. Our solution is reduced to that of Ref. 9 by the transformation $S'(m) = c(m)[1 + S(m)]$.
[19]See, e.g., P. R. Berman, in *Advances in Atomic and Molecular Physics* (Academic, New York, 1978), Vol. 13, pp. 57–112, or P. R. Berman, Phys. Rev. A 13, 2191 (1976).
[20]W. J. Firth, R. Salomaa, and P. E. Toschek, in *Laser Advances and Applications*, edited by B. S. Wherrett, (Wiley, New York, 1980), pp. 107–118.
[21]One could also keep $v$ and $\Delta_{21}$ fixed and search the resonance values for $\Delta_{23}$. This procedure gives the eigenfrequencies of the dressed system.
[22]I. M. Beterov and V. P. Chebotaev, in *Progress in Quantum Electronics*, edited by J. H. Sanders and S. Stenholm (Pergamon, Oxford, 1974) Part 1, Vol. 3, pp. 1–105; see also, C. Delsart and J-C. Keller, J. Phys. (Paris) 39, 350 (1978).
[23]R. Salomaa and S. Stenholm, J. Phys. B 9, 1221 (1976).
[24]B. J. Feldman and M. S. Feld, Phys. Rev. A 12, 1013 (1975); R. Salomaa, J. Phys. B 11, 3745 (1978).
[25]E. Kyrölä and S. Stenholm, Opt. Commun. 30, 37 (1979).
[26]See, e.g., Yu. A. Vdonin, V. M. Ermachenko, and V. K. Matskevich, Kvant. Elektron. (Moscow) 2, 902 (1975) [Sov. J. Quantum Electron. 5, 491 (1975)].